View metadata, citation and similar papers at core.ac.uk

brought to you by CORE

provided by Texas A&M Repository

ACTIVE CONTROL OF UNDERWATER PROPULSOR USING SHAPE MEMORY ALLOYS

A Thesis

by

JONATHAN ALLEN WASYLYSZYN

Submitted to the Office of Graduate Studies of
Texas A&M University
in partial fulfillment of the requirements for the degree of

MASTER OF SCIENCE

December 2005

Major Subject: Aerospace Engineering

ACTIVE CONTROL OF UNDERWATER PROPULSOR USING SHAPE MEMORY ALLOYS

A Thesis

by

JONATHAN ALLEN WASYLYSZYN

Submitted to the Office of Graduate Studies of
Texas A&M University
in partial fulfillment of the requirements for the degree of

MASTER OF SCIENCE

Approved by:

Chair of Committee,	Othon Rediniotis
Committee Members,	Paul Cizmas
	Luis San Andres
Head of Department,	Helen Reed

December 2005

Major Subject: Aerospace Engineering

ABSTRACT

Active Control of Underwater Propulsor Using

Shape Memory Alloys. (December 2005)

Jonathan Allen Wasylyszyn, B.S., Texas A&M University

Chair of Advisory Committee: Dr. Othon Rediniotis

The development of a leading edge propeller blade reconfiguration system using Shape Memory Allow (SMA) muscles is presented. This work describes the design and testing of a leading edge flap, which is used to alter the local camber of a propeller blade. The leading edge flap is deflected by SMA wires housed in the blade and maintained in a fixed position with a shaft locking and releasing mechanism. A locking and releasing mechanism is utilized so that constant actuation of the SMAs is not required to maintain leading edge deflection. The profile at 70% span of the propeller blade was used to create a two-dimensional blade for leading edge flap design implementation and load testing. Deflection of up to five degrees was obtained with the final design of the leading edge flap and locking and releasing mechanism. The SMA muscles used to deflect the leading edge were actuated electronically through resistive heating and were controlled by a proportional/integral gain control algorithm with closed-loop feedback from a linear displacement sensor within the blade. With the final design of the leading edge flap and locking and releasing mechanism, a preliminary design for a three-dimensional propeller was created.

DEDICATION

I would like to dedicate this thesis to my parents Janet and Jeff Edwards for their continued support throughout my college career. Their continual love and understanding allowed me the opportunity to follow my dream and make that dream a reality.

ACKNOWLEDGEMENTS

I would like to thank Dr. Othon Rediniotis for giving me the opportunity to work with him on this propeller project. His extensive knowledge and expertise in experimental research was greatly appreciated throughout the project. I would like to thank Dr. Lance Traub for his technical advice and willingness to assist me throughout the project. I would also like to thank Josh Weimar for his hard work in building the various propeller blade parts and beautiful aluminum leading edge flap.

TABLE OF CONTENTS

Page

ABSTRACT iii

DEDICATION iv

ACKNOWLEDGEMENTS v

TABLE OF CONTENTS vi

LIST OF FIGURES vii

INTRODUCTION 1

Previous Work 1
Smart Material Actuators 3
Shape Memory Alloys 4
Leading Edge Flap 7

EXPERIMENTAL SETUP AND PROCEDURES 8

Leading Edge Flap 8
Experimental Setup for 2-D Blade 25

RESULTS AND DISCUSSION 36

Flow Angularity 36
2-D Blade with Leading Edge Flap 37

PRELIMINARY DESIGN OF 3-D PROPELLER 43

CONCLUSION AND RECOMMENDATIONS 46

Conclusion 46
Recommendations 47

REFERENCES 49

VITA 51

LIST OF FIGURES

Page

Figure 1: Crystal Structure of Nitinol 4

Figure 2: Stress/Temperature Relationship for SMAs 5

Figure 3: Plot of Hysteresis Saturation During SMA Training 6

Figure 4: Cross-Section of Propeller Blade at 70% Span 8

Figure 5: Pressure Distribution for Suction Side in Pascals 9

Figure 6: Pressure Distribution for Pressure Side in Pascals 9

Figure 7: First Leading Edge Locking and Releasing Mechanism Design 10

Figure 8: Actuation of SMA Ring (Tube) Muscle 11

Figure 9: Schematic of Leading Edge Locking and Releasing Mechanism 12

Figure 10: Design of Leading Edge Locking and Releasing Mechanism 12

Figure 11: SMA Based Locking and Releasing Actuation Mechanism 14

Figure 12: Locking and Releasing SMA Actuator 14

Figure 13: Leading Edge Locking and Releasing Mechanism 15

Figure 14: Top and Bottom Leading Edge Pieces 15

Figure 15: Surface of Leading Edge Pieces 16

Figure 16: Inside of Aluminum Top and Bottom Leading Edge Pieces 17

Figure 17: Leading Edge Actuation Schematic 18

Figure 18: First Prototype of Flap with SMA Actuators and Approximate Location 18

Figure 19: First Prototype SMA Actuation Setup 19

Figure 20: Trailing Edge Cavity 20

Page

Figure 21: Trailing Edge and Insert 20

Figure 22: SMA Strips and End Connections 21

Figure 23: Complete Leading Edge Actuation System 22

Figure 24: Redesigned Trailing Edge Cavity 23

Figure 25: Schematic of Leading Edge Actuation System 23

Figure 26: SMA Strips and End Connections 24

Figure 27: Complete Redesigned Leading Edge Actuation System 24

Figure 28: Aerospace Department's SMA Training Apparatus 25

Figure 29: Schematic of Water Tunnel Setup 27

Figure 30: Side View of Acrylic Inserts with Fairing and Endplates 28

Figure 31: Through View of Acrylic Inserts with Fairing and Endplates 28

Figure 32: Balance with Sting 30

Figure 33: Top View of Water Tunnel Balance 30

Figure 34: Schematic of Experimental Setup 31

Figure 35: Microstrain DVRT Sensor 33

Figure 36: Lift vs. Angle of Attack for NACA 0012 36

Figure 37: 2-D Blade in Water Tunnel During Testing 38

Figure 38: Lift vs. Angle of Attack of 2-D Blade for Increasing Flap Deflection (Def) .. 39

Figure 39: Drag vs. Angle of Attack of 2-D Blade for Increasing Flap Deflection (Def) 39

Figure 40: Leading Edge at 0.0 Degrees (Left) and -2.5 Degrees (Right) 41

Figure 41: Positive Deflection Trace of Leading Edge Flap 42

Figure 42: Negative Deflection Trace of Leading Edge Flap 42

Page

Figure 43: 3-D Rendering of Propeller, Pressure Side 44

Figure 44: 3-D Rendering of Propeller, Suction Side..... 44

Figure 45: Aluminum and Phenolic Slip Rings 45

INTRODUCTION

Previous Work

Surface ships and underwater vehicles of today generally utilize one of two basic propeller designs. The most common design is the fixed geometry propeller. This propeller is designed to obtain its greatest performance at the vessel's primary operating conditions. The propeller is highly susceptible to cavitation and produces noise and acoustic signatures, which can hinder a military vessel's ability to move through the water with stealth. The second design is the controllable pitch propeller. The blades of the propeller are able to rotate at the hub interface to change their pitch[1]. Controllable pitch propellers typically use hydraulics or complicated mechanical systems, located in the hub, to perform the blade rotation. The change in pitch allows for a wider range in operating conditions, but is limited by the performance characteristics of the propeller blade at different angles of attack. With both propeller designs having fixed blade geometries, limitations, which are common in most passive control systems, are introduced. One of the limitations is the loss of performance in off-design conditions, such as when a vessel performs a maneuver. Due to this loss of performance, there arises opportunity to develop active propeller geometry reconfiguration systems to enhance a propeller's performance.

Several recent studies have been conducted to improve propeller performance using geometry reconfiguration systems that require little or no mechanical work. In one study, the reduction in radiated noise due to a decrease in the rotational speed of the

---

This thesis follows the format of the *AIAA Journal.*

propeller was considered[2-3]. In this study a small biomimetic propeller with the aft sections of its blades made of artificial muscles (electroactive polymeric sheets) was built and tested. It was shown that the muscles could be used to increase cambering in order to increase the lift force. This increased lift would allow for a slower rotational speed of the propeller at the normal operating condition, which would in turn reduce the radiated noise. Active blade cambering could be used to change blade loading during off-design conditions to improve the performance of a propeller.

Another study by Quackenbush et al. addresses the problems encountered during low speed maneuvering and control surface deflection[4-5]. Current systems for turning and maneuvering of vessels are limited to rudders and sternplanes. These control surfaces can create noise due to interaction with the propeller wash generated upstream, and at low speeds tend to be ineffective. Quackenbush et al. have proposed a design for a steerable ducted propeller, which is actuated by Shape Memory Alloys (SMAs)[4-5]. SMAs are used to augment the aft portion of the duct to redirect the propeller wash and yield a direct steering force. The ducted propeller has been successfully tested in both benchtop and in-water environments. Water tunnel tests of the ducted propeller are currently being conducted. Quackenbush et al. states that the potential advantages of this steering control technology include: enhanced low speed maneuvering, reduction or elimination of conventional steering surfaces and of associated actuator noise, and elimination of hydraulic actuation hardware[4]. An active cambering system could change the characteristics of the propeller wash upstream of a control surface to reduce both noise and excitation of structural modes on the control surface.

A study on propellers examines the radiated noise caused by non-uniform wake across a propeller[6]. This study proposes the possibility of using a reconfigurable upstream stator, guide-vane or control appendage to generate a non-uniform wake in order to alter the noise signature instead of suppressing it. In the work, it was shown that the fluctuation in lift produced by a rotor could be modified beneficially by altering the wake characteristics of an upstream stator. Active blade cambering can be utilized to change the acoustic signature of a propeller for masking the movement of military vessels.

Smart Material Actuators

The propellers of today have thin blades and usually large amounts of twist. With these geometric constraints, typical actuation systems, such as hydraulics or mechanical motors, are too large and too complex to be housed within the blades and used for means of blade geometry reconfiguration. The limited space available within the blades gives the opportunity for use of a relatively new actuator technology, which uses active or "smart" materials. Many studies have been conducted to assess the use of smart material as actuators in mechanical systems. The use of smart material in helicopter rotor blades is a major area of interest at this time[7-9]. Other applications include the use of smart materials in the sternplane of submarines[10] as control surface deflection tabs and linear actuators in biomimetic hydrofoils[11-12]. The material chosen in many of these studies and research applications is the Shape Memory Alloy (SMA). This material is attractive due to its small size and capability of producing large strains, up to 4% for two-way training, and large actuation forces. Other SMA advantages are simplicity of actuation system, low voltage requirements and silent actuation. SMAs can be actuated electrically through

computer algorithms[13] using resistive heating with relatively low voltages and no recognizable acoustic signature[11-12]. SMA actuation does have its disadvantages. Currently SMAs have low energy efficiency and relatively large current requirements and can experience actuation loss and fatigue over repetitive cyclic loading[11-12].

Shape Memory Alloys

The first SMA to be discovered (and the one used in this experiment) is Nitinol by William J. Buehler in 1961. The name comes from the two elements used in its creation, Ni and Ti, and the abbreviation of the Naval Ordinance Laboratories (NOL) where it was discovered[14]. SMAs are metals that have two unique properties, pseudo-elasticity and the shape memory effect[15]. The shape memory effect is the driving mechanism for most SMA actuator systems designed today. The shape memory effect is made possible through a change in the crystal structure of the material between the martensite and austenite phase. A depiction of the two crystal structures can be seen in Figure 1.

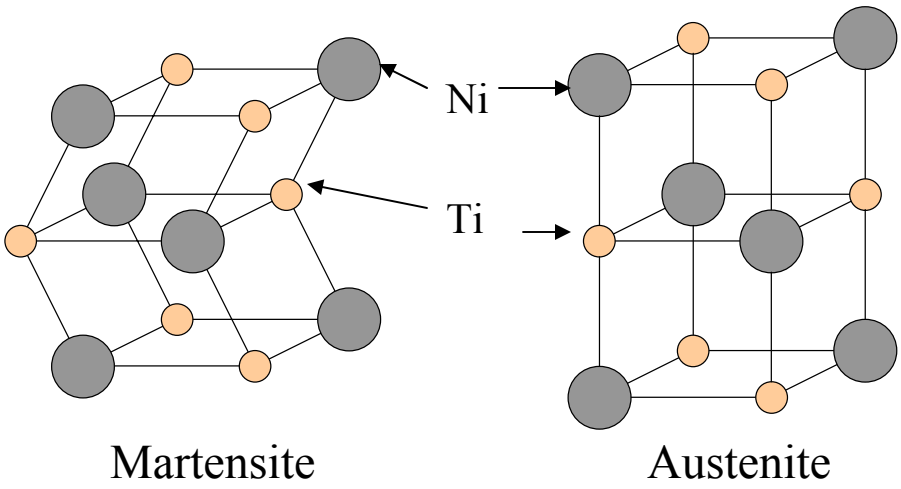

Figure 1: Crystal Structure of Nitinol

In the martensite phase, which exists at lower temperatures, the material is relatively soft and easy to deform. In the austenite phase, existing at higher temperatures, the crystal structure becomes cubic and rigid. The amount of martensite or austenite in the material depends on the stress and temperature of that particular piece. Figure 2 shows a qualitative plot of the stress/temperature relationship for the two phases.

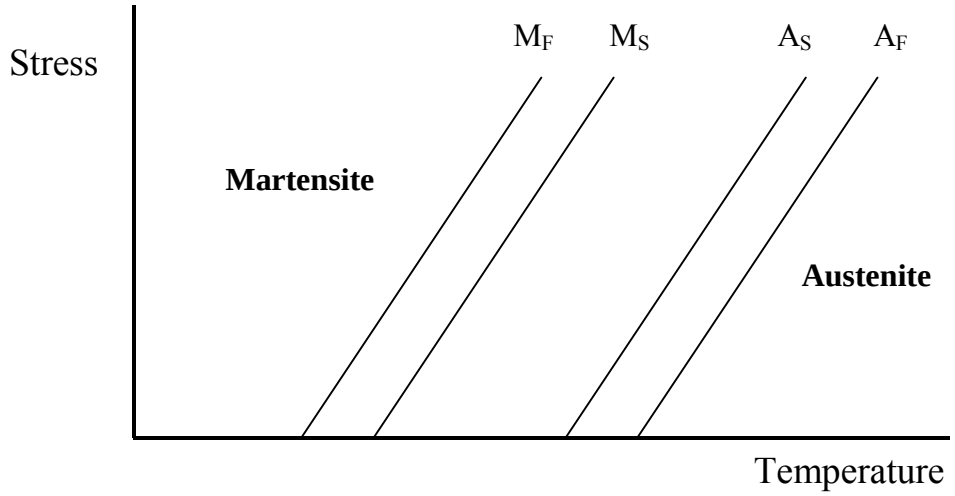

Figure 2: Stress/Temperature Relationship for SMAs

As shown in Figure 2, left of martensite finish, M_F, only martensite is present within the material. To the right of austenite finish, A_F, austenite is the only phase present. The two phases can coexist if the stress and temperature are such that the material falls within M_F and A_F. If an SMA is below the martensite finish temperature and is deformed, the original shape can be recovered by heating the material above the austenite finish temperature. To utilize SMAs as mechanical actuators, training of the material must be performed. Untrained SMAs have unpredictable actuation characteristics, which is not desirable for mechanical systems. One common training method is two-way training. For two-way training, stress is applied to the SMA and 50

thermal cycles are performed to saturate the hysteresis curve, which is a plot of the actuation stroke vs. temperature of the material. The stress applied during the training is usually greater than the stress anticipated during normal actuation to prevent retraining while in operation. The end result is an SMA that will expand a certain length, depending on the amount of stress used in training, in the martensite phase without a load on the wire. Figure 3 shows an example of the saturation of a hysteresis curve for an SMA trained at Texas A&M University.

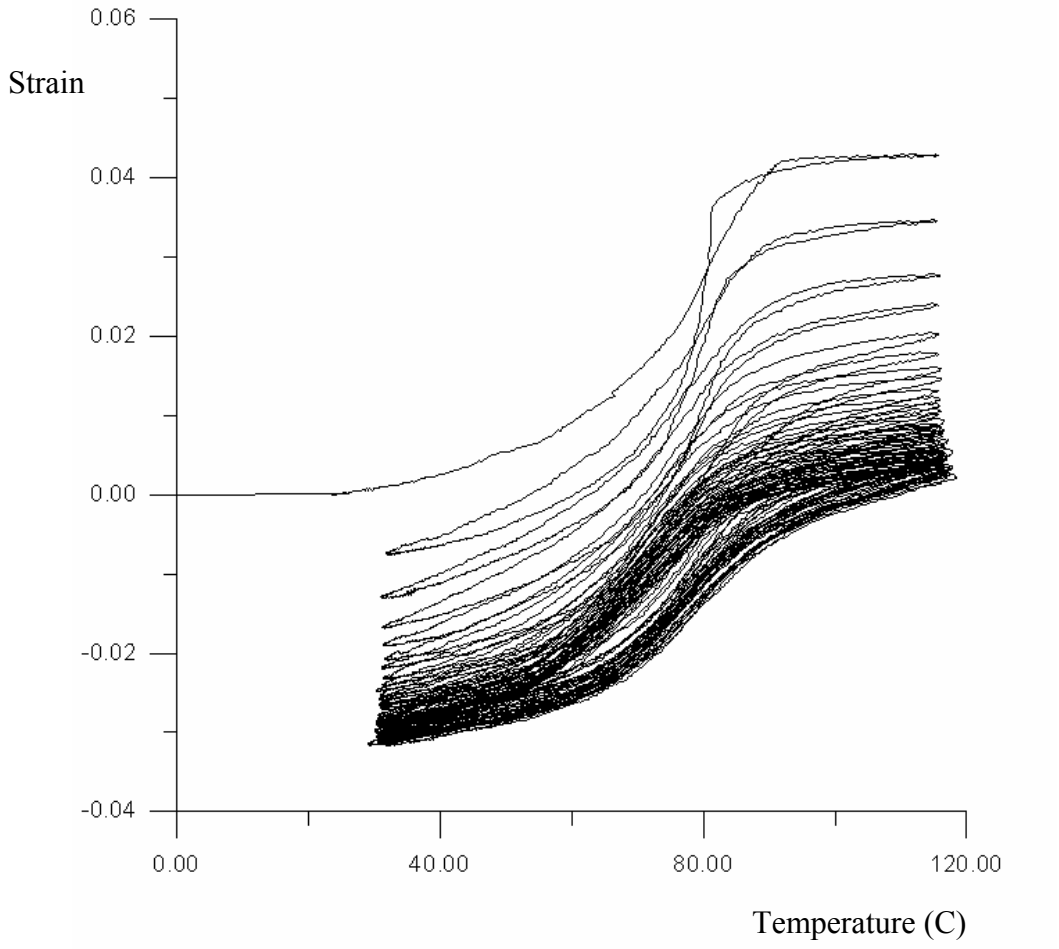

Figure 3: Plot of Hysteresis Saturation During SMA Training

Leading Edge Flap

This thesis presents the design and implementation of a leading edge flap actuated by SMAs for active cambering of individual propeller blades. When deflected, a leading edge flap will change the local camber of the blade and in turn change the lift generated, much like a leading edge flap on an airplane wing. The flap was designed with an internal shaft locking and releasing mechanism so that constant actuation of the SMAs was not required for leading edge deflection. A bench test of possible designs was performed to validate their effectiveness in achieving the goals of leading edge deflection and shaft locking. The most promising designs were then implemented into a two-dimensional (2-D) blade that spanned 0.2032 meters with the profile of the propeller blade at the 70% span location. Load cell data was collected on the 2-D blade for different leading edge deflection and angle of attack combinations using a water tunnel and 2-axis balance. Using the final design of the leading edge flap and locking and releasing mechanism, a preliminary design for a three-dimensional (3-D) propeller was created.

EXPERIMENTAL SETUP AND PROCEDURES

Leading Edge Flap

A leading edge flap was designed for implementation in a 2-D blade and eventually a 3-D propeller blade. The cross-section of the Northrop Grumman Newport News propeller blade at 70% span was used for the profile shape of the 2-D blade, which can be seen in Figure 4.

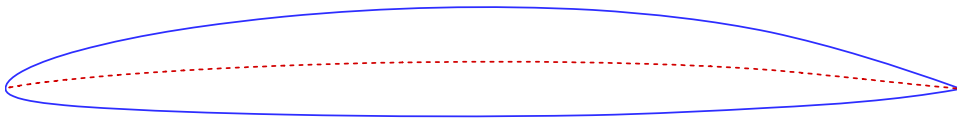

Figure 4: Cross-Section of Propeller Blade at 70% Span

Computational Fluid Dynamics (CFD) analysis was performed on the Northrop Grumman Newport News propeller blade by graduate research assistant Joaquin Gargoloff using Fluent. The calculations were performed with the blade stationary and the fluid rotating at 382 revolutions per minute using a rotational reference frame. The inlet total pressure was 316,300 Pa with a static pressure of 310,200 Pa. Figures 5 and 6 show the surface pressure results from CFD for both the suction and pressure side of the blade respectively. The cross-section at 70% span was chosen due to the low-pressure region located on the suction side toward the tip of the blade. This low-pressure region gives the ideal location for a leading edge flap. A leading edge flap in this region would allow for the largest possible variation in blade loading and in turn the largest changes in propeller performance.

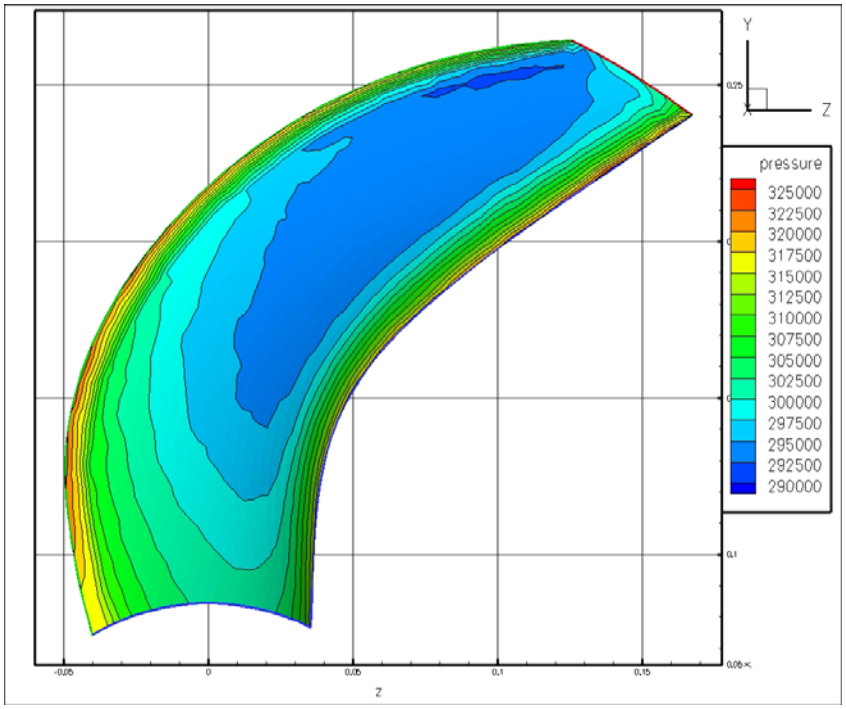

Figure 5: Pressure Distribution for Suction Side in Pascals

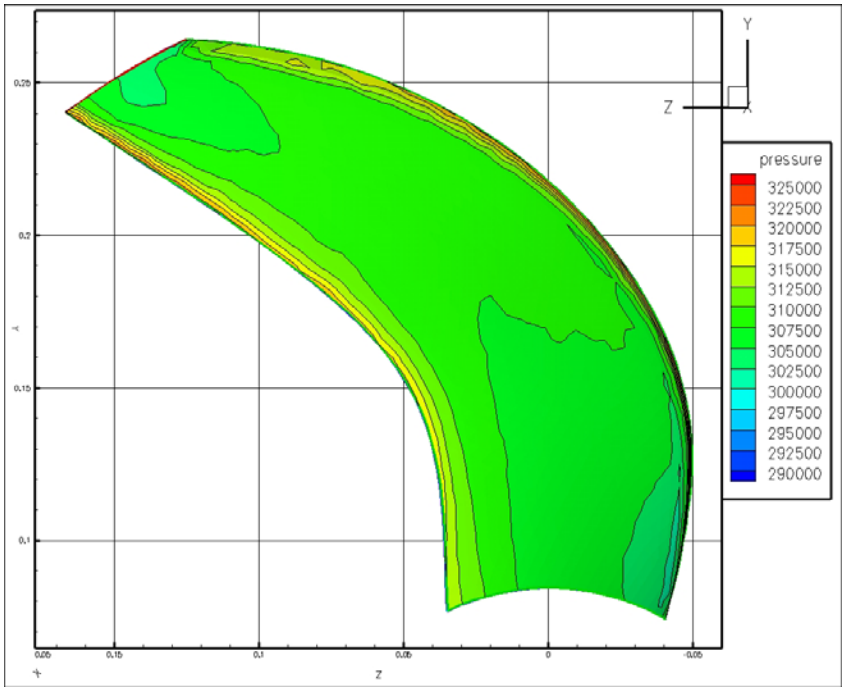

Figure 6: Pressure Distribution for Pressure Side in Pascals

The original chord length of the blade cross-section was doubled to a length of 0.1163 meters to ensure that everything needed to actuate the leading edge could be contained within the propeller. The hinge point was located at the quarter-chord, and the span of the 2-D blade was chosen to be 0.2032 meters with the leading edge flap extending the complete span.

Locking and Releasing Actuation Mechanism

The leading edge flap was designed with an internal chamber to house a locking and releasing SMA muscle. Between actuations, the leading edge flap "grips" onto a shaft (shaft diameter slightly larger than the hole it goes through) and is thus locked in place to prevent rotation. When actuation (leading edge deflection) is imminent, the muscle in the internal chamber is actuated and the grip/locking is released. After the leading edge flap is deflected to its desired new angle (by the main SMA actuator), the locking and releasing SMA muscle is relaxed, and the leading edge flap is locked in place again by the clamping force. Figure 7 shows the first design of the leading edge locking and releasing mechanism. The actuator was a ring (tube) SMA.

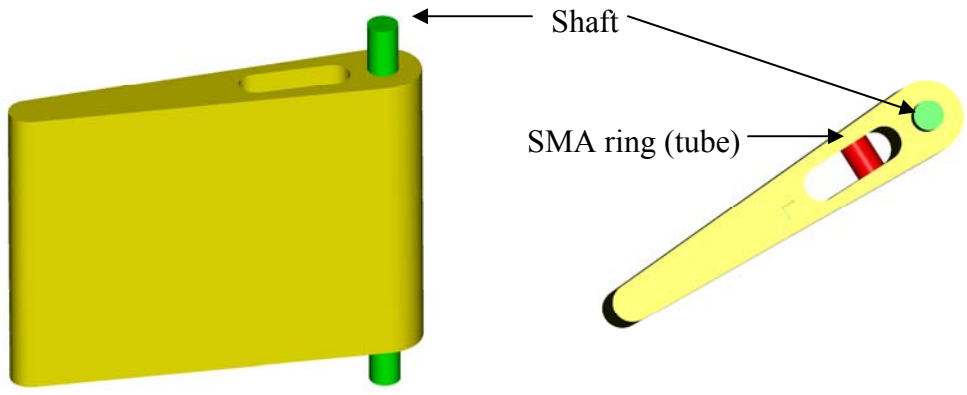

Figure 7: First Leading Edge Locking and Releasing Mechanism Design

When the SMA ring is actuated, its diameter shrinks by 2 % and the length increases by 2 %. Figure 8 shows the actuation of an SMA ring muscle. Both ends of the SMA ring were to push the blade walls apart and release the grip/shaft during actuation. After leading edge deflection, the SMA ring muscle would be cooled to martensite and the blade would lock on the shaft by the blade walls' restoring force as described above.

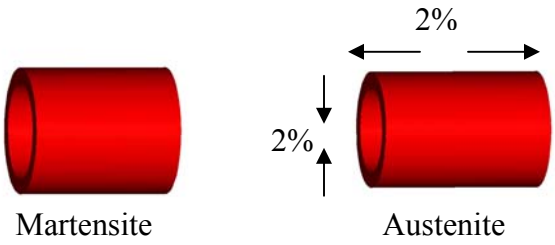

Figure 8: Actuation of SMA Ring (Tube) Muscle

Due to the difficulty in wiring the SMA ring, the locking and releasing actuation mechanism was redesigned to utilize an SMA strip. The second locking and releasing actuator design is shown in Figure 9 and Figure 10. As the SMA muscle is actuated (muscle shrinks in length), a muscle terminal (oval component in Figure 9 middle) pushes the blade walls apart, thus deflecting them and releasing the grip (Figure 9, lower). The walls need to be deflected apart only by a couple thousands of an inch in order for the grip to be released. Therefore, given SMA's available actuation strain (as high as 4%), only a small length of SMA strip was required.

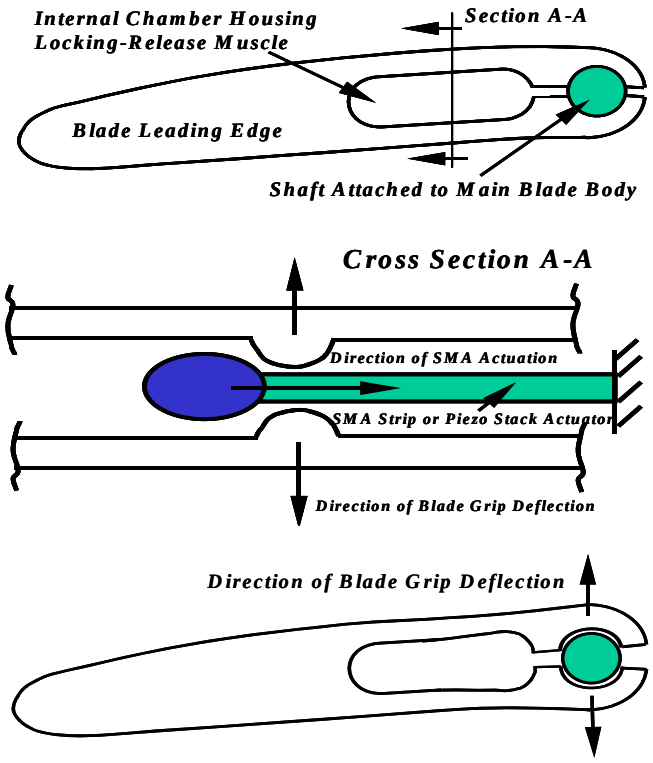

Figure 9: Schematic of Leading Edge Locking and Releasing Mechanism

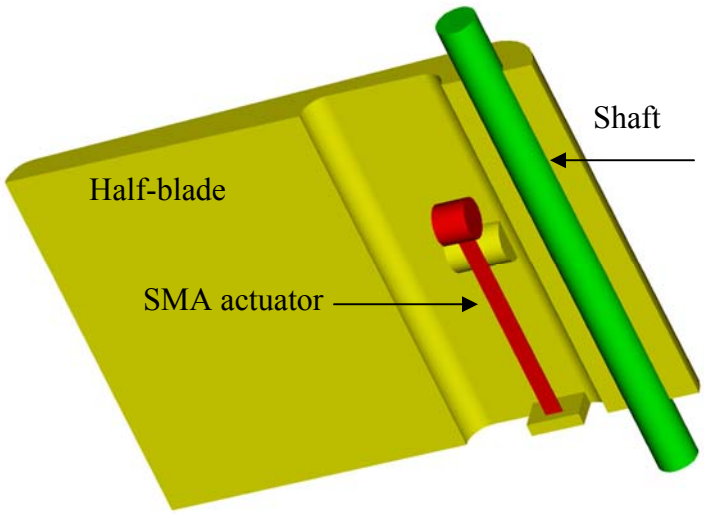

Figure 10: Design of Leading Edge Locking and Releasing Mechanism

For the first prototype, two aluminum half-blade pieces were manufactured to represent the leading edge flap. Small screws were used to secure two half-blade pieces together and exert a clamping force on the shaft. The clamping/gripping force generated by the screws was large enough to withstand the calculated hydrodynamic moment and flap restoring moment. For the typical dimensions and operating conditions of the propeller design obtained from Newport News Shipbuilding, the necessary moment that the locking and releasing mechanism had to withstand was calculated to be 210 Nmm. The moment was reproduced, in this first prototype by hanging a weight of 0.850 kg from the flap at a distance of 25 mm from the shaft/flap pivot axis. The gripping force can actually withstand up to a 1.3 kg weight at this distance, which is equivalent to a moment of 319 Nmm. Figures 11 and 12 show the locking and releasing SMA actuator prototype based on Figure 9. A K-alloy (NiTiCu) SMA strip was utilized as the SMA actuator. The size of the strip was 0.9 mm x 2.5 mm x 30 mm in length. A screw connected to one end of the SMA strip is used to prestrain the SMA and ensure that contact is made with the blade walls and muscle terminal. The kinematics, contact angles and contact forces between the muscle terminal and the blade walls, have been designed such that during the muscle relaxation phase the terminal is not “wedged” between the blade walls, rather it is pushed out of the way.

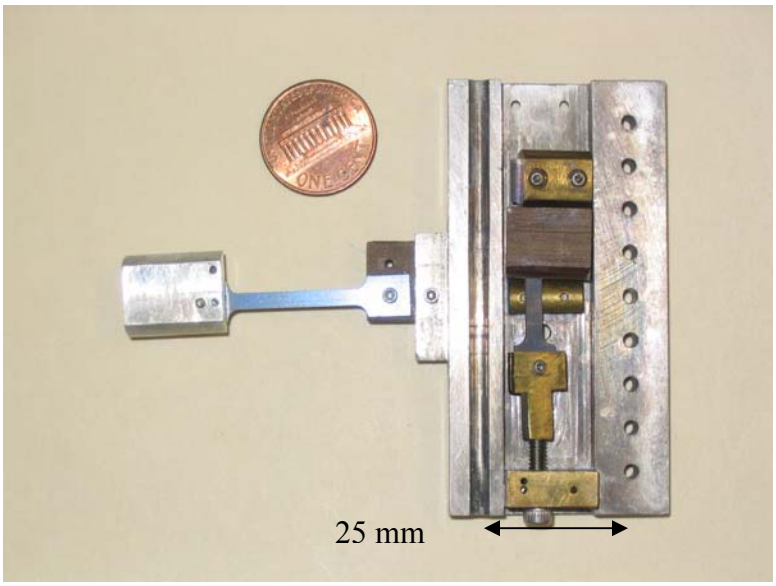

Figure 11: SMA Based Locking and Releasing Actuation Mechanism

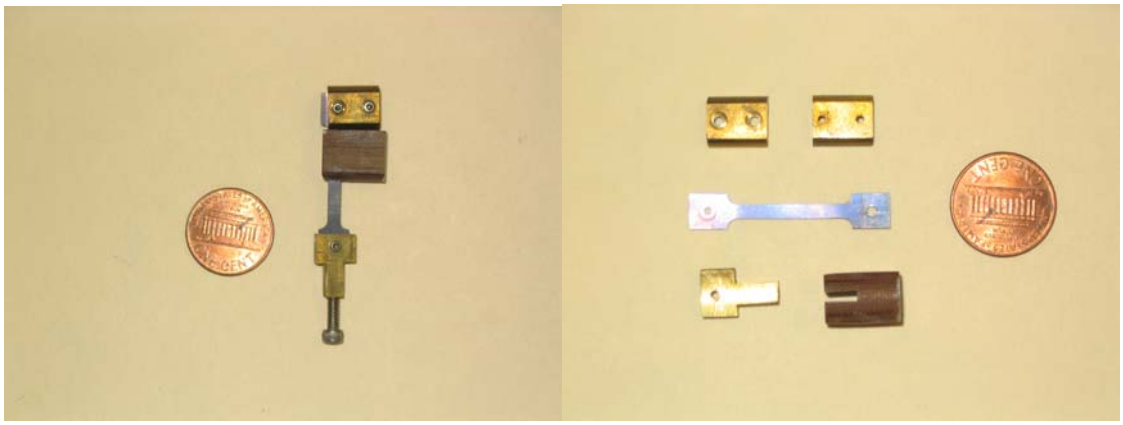

Figure 12: Locking and Releasing SMA Actuator

For the implementation into the 2-D blade, the locking and releasing mechanism of the leading edge is identical to that stated above for the prototype. The leading edge has an internal chamber, which contains an SMA strip. When actuated, the SMA strip releases the clamping force on the shaft and allows the leading edge to be moved with less effort. The SMA strip is actuated electronically through resistive heating. Electrical connection points were incorporated at each end of the SMA strip for the installation of

the wires. Figure 13 shows the leading edge locking and releasing mechanism of the 2-D blade.

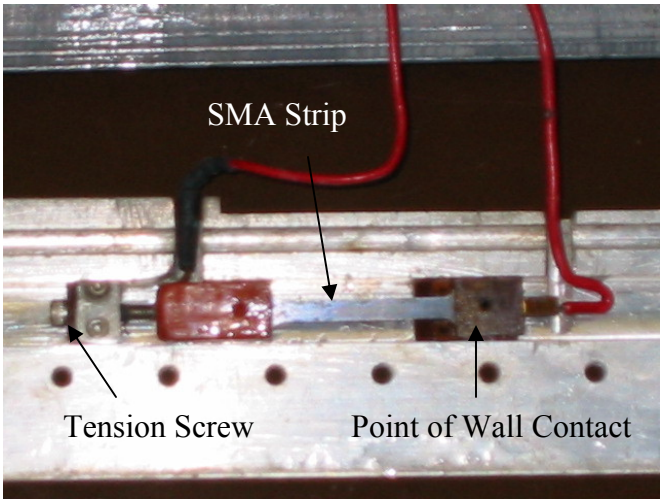

Figure 13: Leading Edge Locking and Releasing Mechanism

The leading edge flap is made of two pieces, a top and bottom, so that the locking and releasing mechanism can be installed and then accessed if needed. Figure 14 shows a 3-D rendering of the top and bottom leading edge pieces designed for the 2-D blade, which are 0.2032 meters in length.

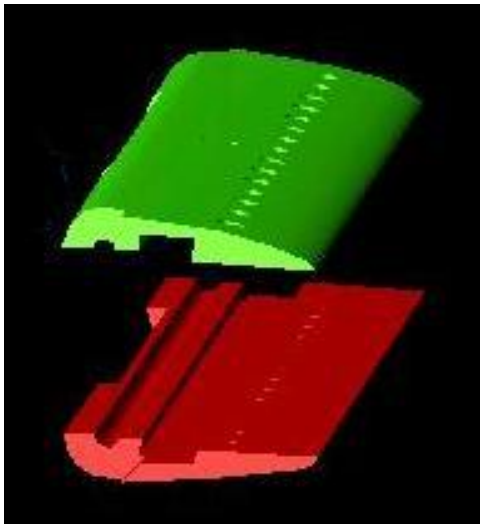

Figure 14: Top and Bottom Leading Edge Pieces

The two leading edge pieces are held together by counter sunk screws that run the span of the blade. As stated earlier, these screws provide the clamping force needed to lock the leading edge on the shaft. To ensure that the two leading edge pieces could withstand the clamping force required, they were made out of aluminum. There are a total of fifteen screw holes that run the span of the leading edge. The large number of screw holes was necessary for the fabrication and attachment of the two aluminum leading edge pieces, as well as to generate the needed clamping force. Figure 15 shows the outside surface of the top and bottom leading edge pieces that were machined using a Computer Numerical Control (CNC) mill.

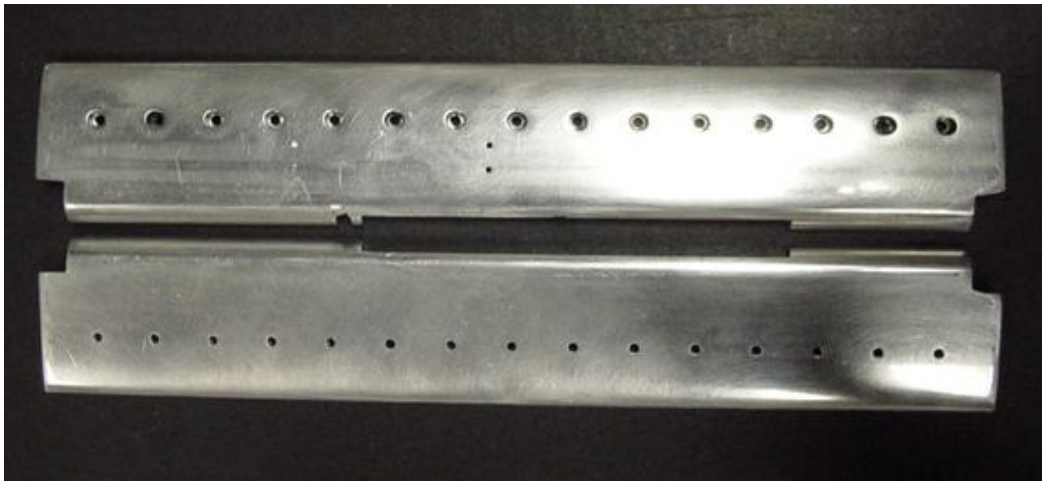

Figure 15: Surface of Leading Edge Pieces

Grooves were milled into the top leading edge piece so that wires can be run from the trailing edge to the SMA strip within the leading edge flap. The inside of the leading edge pieces that have been milled out of aluminum can be seen in Figure 16.

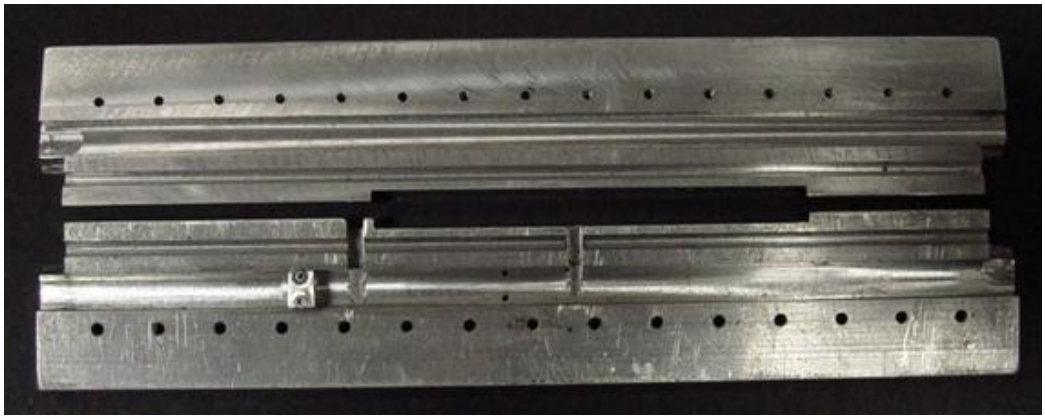

Figure 16: Inside of Aluminum Top and Bottom Leading Edge Pieces

Leading Edge Actuation Mechanism

As mentioned earlier, with propellers having thin blades and large amounts of twist, typical actuation systems are too large and complex. This confined space makes SMAs ideal for the current application. The fact that the SMA actuators can generate ample actuation load allows for a simplified design, which entails having two SMA muscles (one for each deflection direction). Figure 17 illustrates the concept for the main leading edge SMA-based actuation system. At the non-actuated state, length of actuator I and II are l. If SMA actuator I is actuated to $l - \alpha$, the blade is deformed as shown in Figure 18. To return to its original shape, SMA actuator I is deactivated and if it does not return on its own, SMA actuator II is activated to bring the leading edge back. For the first design, two K-alloy SMA strips were utilized as actuator I and actuator II. The size of each strip was 0.9 mm x 2.5 mm x 26 mm in length.

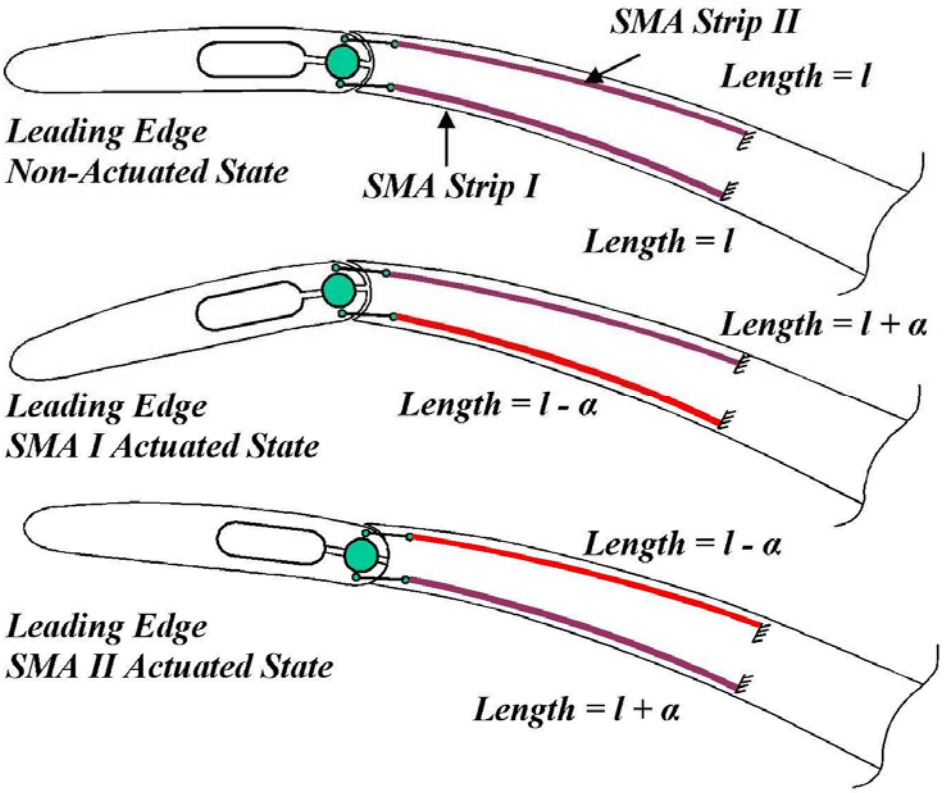

Figure 17: Leading Edge Actuation Schematic

Figure 18 shows the approximate location of the leading edge flap and the design of the prototype leading edge flap with SMA actuators attached.

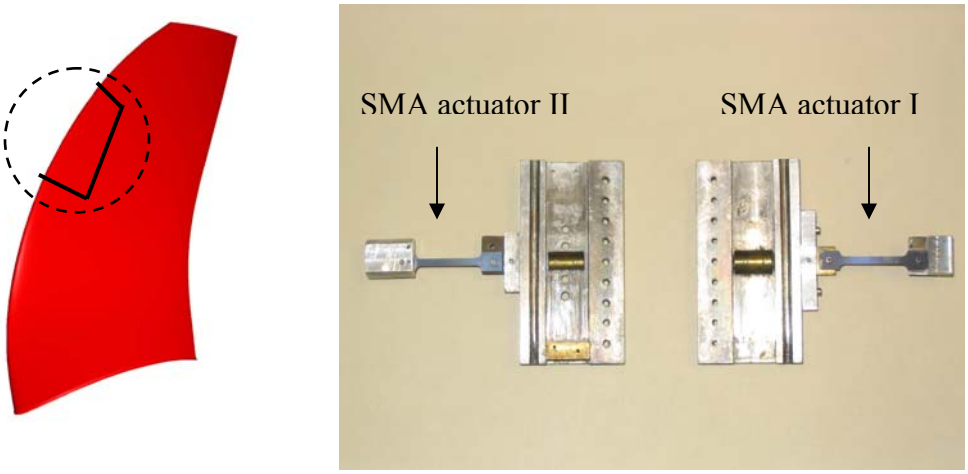

Figure 18: First Prototype of Flap with SMA Actuators and Approximate Location

Figure 19 left, shows the first prototype of the active flap with SMA actuators I and II clamped onto the test frame. Initial experiments were performed with the first prototype with flap deflections of up to 10 degrees being achieved. Figure 19 right, shows the leading edge deflected. At this phase, the actuation of the SMAs was achieved via hot water.

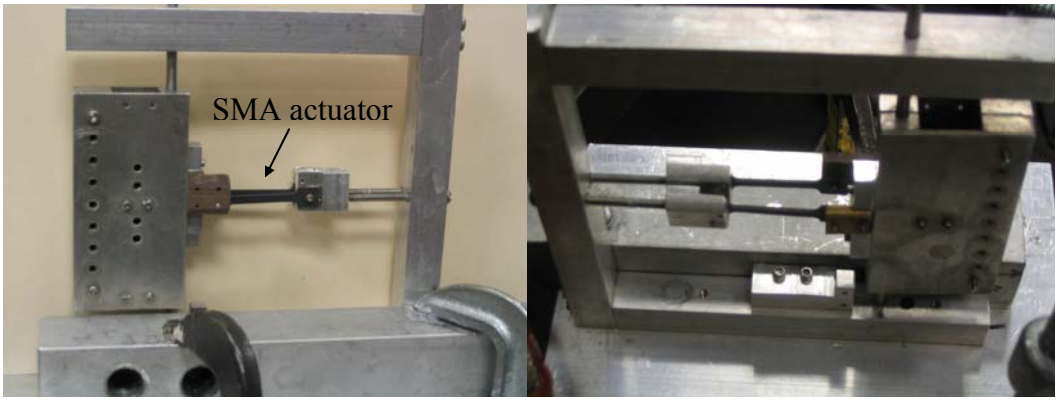

Figure 19: First Prototype SMA Actuation Setup

The trailing edge of the 2-D blade was designed with an empty cavity that is 0.1016 meters in the span wise direction and approximately 0.0635 meters in the chord wise direction. The cavity houses the SMAs and sensor used for the actuation of the leading edge. Figure 20 shows a 3-D rendering of the original trailing edge cavity. The 2-D blade is 0.2032 meters in span with a 3.175 mm diameter steel shaft located at the hinge point.

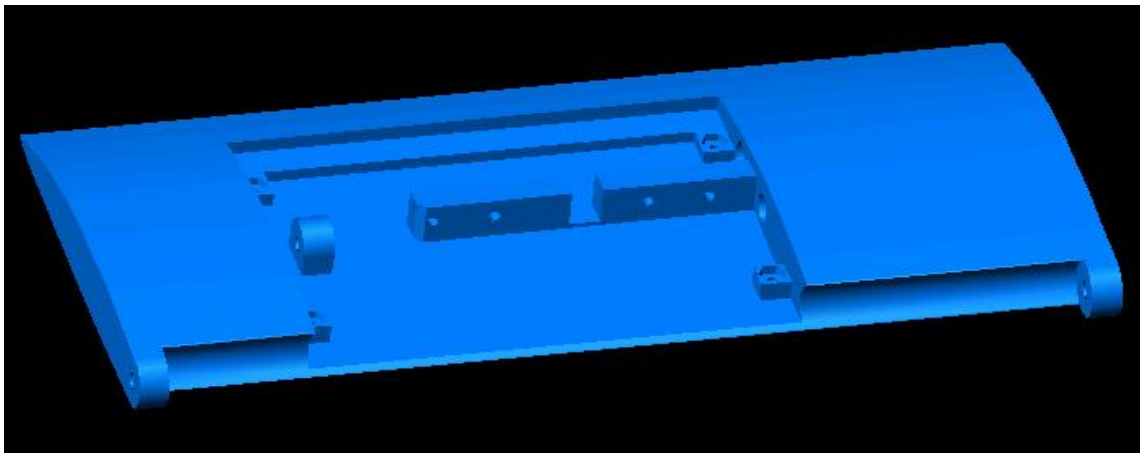

Figure 20: Trailing Edge Cavity

The blade has an insert on the top surface of the trailing edge for access to the cavity. The insert is fastened to the trailing edge by the use of screws. A 3-D rendering of the trailing edge and top surface insert are shown in Figure 21. Both the trailing edge and insert were made of Acrylonitrile-Butadiene-Styrene (ABS) plastic using a rapid prototype machine.

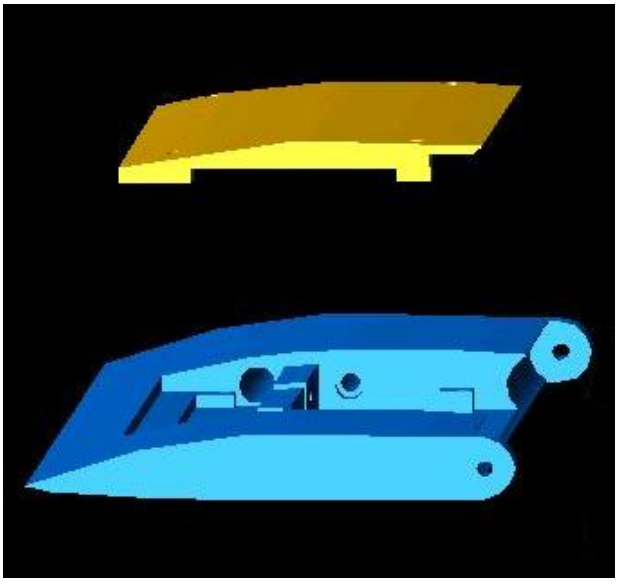

Figure 21: Trailing Edge and Insert

A hole 9.525 mm in diameter protrudes through the side of the blade into the cavity to allow the running of wires from outside the water tunnel to the SMAs and sensor. For the load experiment, the blade was not watertight so that the surrounding water could be used for the cooling of the SMAs. The ends of the wires used to deliver power were soldered to brass tabs. The brass tabs were sandwiched between the SMA strips and hinges made of Phenolic, a strong nonconductive material. One hinge of an SMA was connected to the leading edge by screws while the other end was connected to a small aluminum block. With the hinges connected to the leading edge pieces, the SMAs maximum moment arm is 3.34 mm. Figure 22 shows the SMA strips attached to the aluminum blocks and hinges.

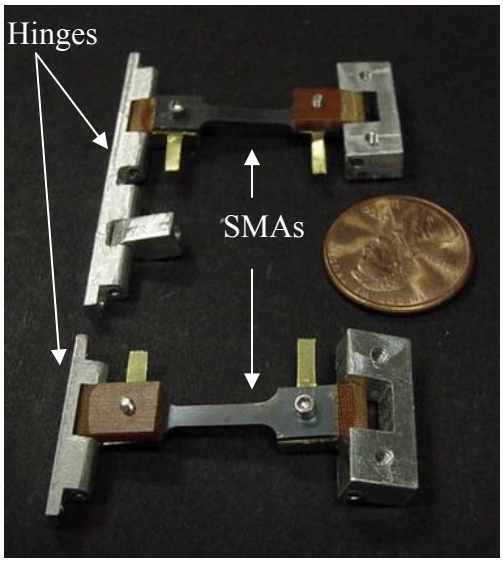

Figure 22: SMA Strips and End Connections

The aluminum blocks were secured to the trailing edge by the use of screws. By tightening the screws, tension would be applied to prestrain the SMA strips. A complete setup of the original leading edge actuation system can be seen in Figure 23.

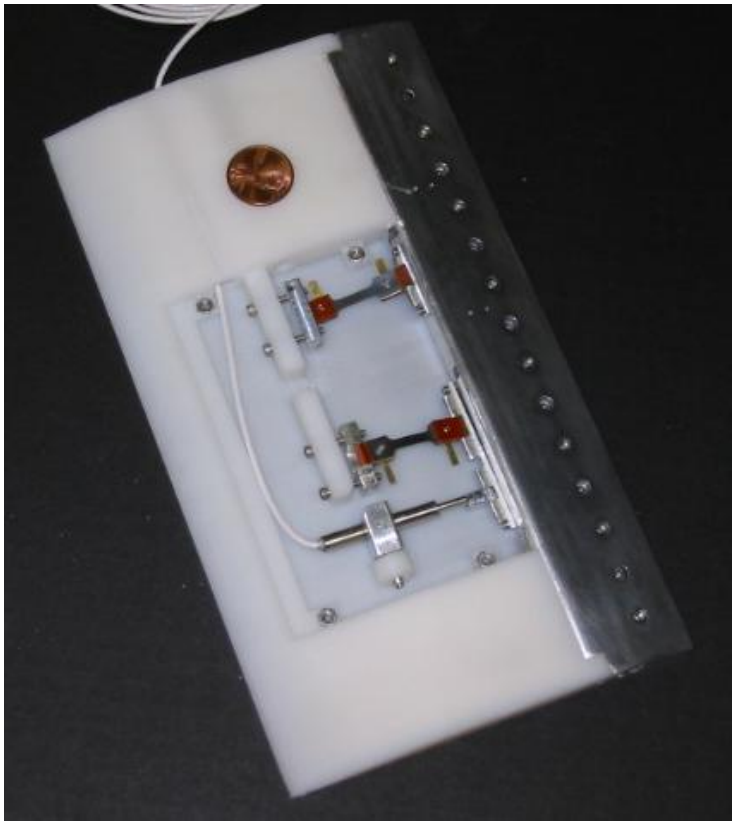

Figure 23: Complete Leading Edge Actuation System

The trailing edge of the 2-D blade was redesigned to house a different SMA actuator than was previously used for leading edge deflection. It was found that the SMA strips described earlier required too much power to actuate with the two SMAs working against one another (antagonistically). Another problem was that the blade's size and rigidity was not adequate to withstand the strain from the two SMAs while under actuation. To eliminate the problems, SMA wire was substituted for the strips and the blade cavity was redesigned adding material in the open areas to reinforce the blade. Figure 24 shows a 3-D rendering of the redesigned trailing edge cavity.

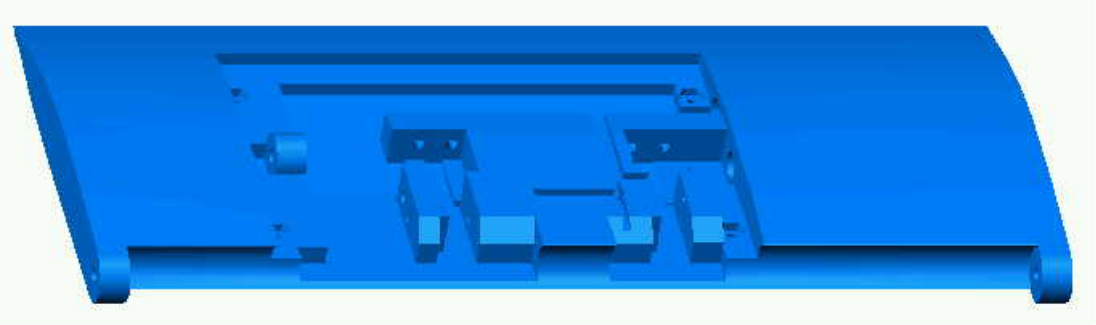

Figure 24: Redesigned Trailing Edge Cavity

In the new design, aluminum hinge pieces are held on each end of the SMA wires by pressure exerted from screws. The electrical wires used to power the SMAs are soldered to brass tabs and the tabs are connected to the hinge pieces using the screws. The aluminum hinges have pins made of Phenolic to insulate the rest of the blade from the electricity. One hinge of an SMA is connected to the leading edge while the other end is connected to the trailing edge. An aluminum pulley between the two hinges is used to apply the needed tension for prestrain of the SMAs and for making any adjustments for zeroing the leading edge angle. Figure 25 shows a schematic of the leading edge actuation system using SMA wires. The aluminum pulley is secured to the trailing edge by the use of screws. By adjusting the screws, the tension can be increased or decreased. Figure 26 shows the SMA wires attached to the aluminum hinge pieces with the pulleys applying tension.

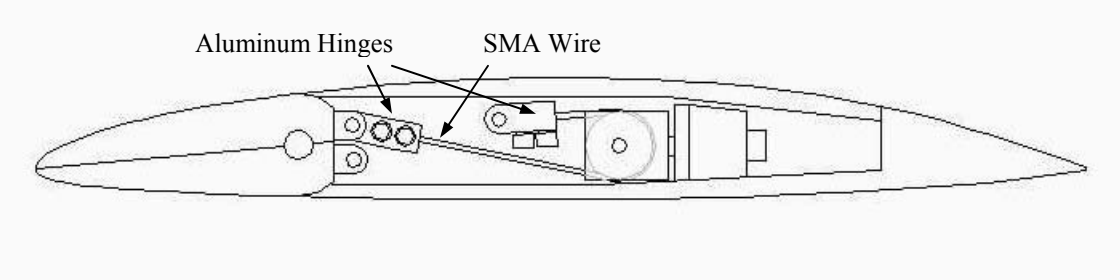

Figure 25: Schematic of Leading Edge Actuation System

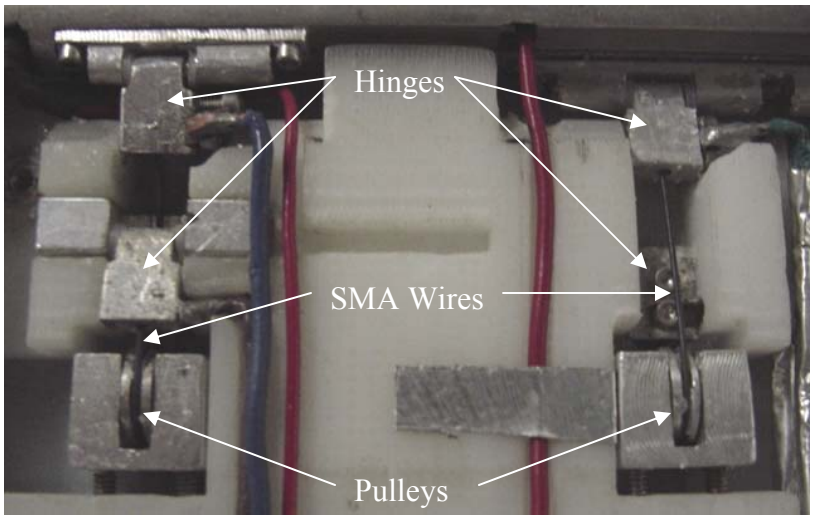

Figure 26: SMA Strips and End Connections

A complete setup of the redesigned leading edge actuation system can be seen in Figure 27. With the complete setup, the maximum moment arm for leading edge actuation is 3.34 mm.

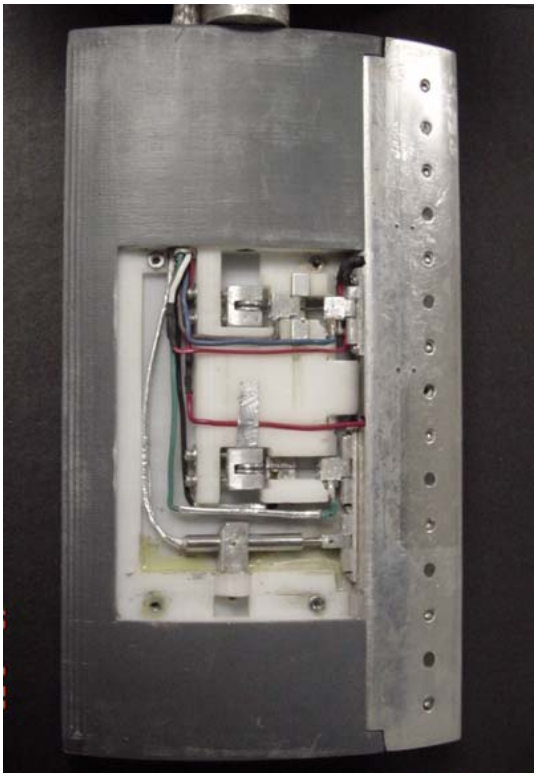

Figure 27: Complete Redesigned Leading Edge Actuation System

Experimental Setup for 2-D Blade

Training of SMAs

The SMA wires used to deflect the leading edge and SMA strip located within the leading edge used to reduce the clamping force are NiTi-Cu with 10% copper. These SMAs are also known as K-alloy and were purchased from SMA Incorporated. The SMA wires have a diameter of 0.6858 mm. Before training of the SMAs began, they were placed in an oven at 450°C for a period of 20 minutes to relieve any residual stress that may reside within the material. The wires and strip were then trained using the Texas A&M University, Department of Aerospace Engineering's SMA training apparatus (Figure 28). The apparatus contains a Linear Voltage Displacement Transducer (LVDT) to measure movement of the applied load while the SMA is actuated.

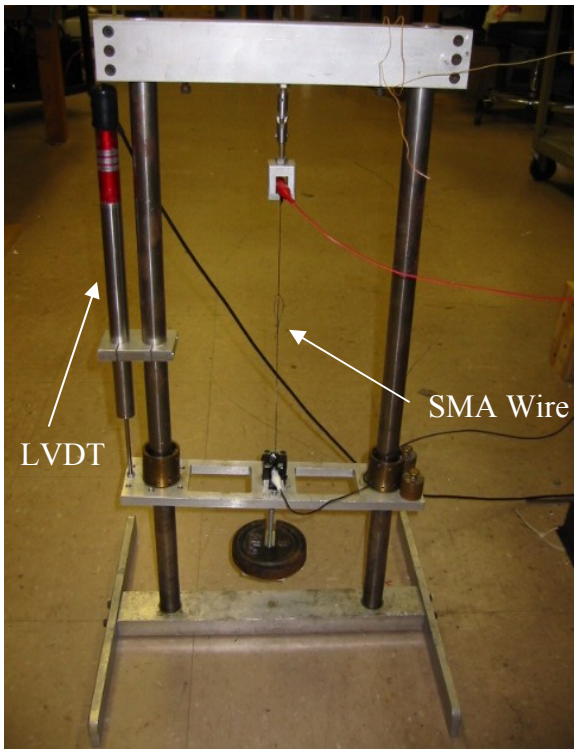

Figure 28: Aerospace Department's SMA Training Apparatus

During training, a weight of approximately 142 Newtons (N) was hung from the SMAs to produce a stress of 400 Mega-Pascals (MPa). The SMAs were put through 50 thermal cycles to ensure full saturation of the hysteresis curve. A thermocouple was attached to the SMAs for temperature readings. The training program uses the temperature from the thermocouple and preset temperature limits to control the thermal cycles. The actuation stroke of the SMAs was recorded using the LVDT through all 50 thermal cycles. The SMA wires obtained a two-way strain of approximately 3% during the process. The stress of 400 MPa used in the training is larger than the stress the SMA wires were expected to encounter during actuation of the leading edge. This larger stress was used to ensure that the problem of retraining the SMAs during actuation did not occur.

Water Tunnel

To prepare for the experiment on the 2-D blade, modifications had to be made to the water tunnel housed at the Texas A&M University, Department of Aerospace Engineering. The water tunnel is an Eidetics Model 2436, which holds 18,927.06 liters of water and has a 0.6096 m x 0.9144 m x 1.8288 m glass test section. The water tunnel is powered by a Baldor 25-hp electric motor and with the cross-section specified above allows for a maximum velocity of approximately 1 m/s. To be able to obtain reliable data from the test run of the 2-D hydrofoil, the cross-section of the water tunnel was reduced from 0.6096 m in width to 0.3048 m using acrylic wall inserts. Figure 29 shows a schematic of the water tunnel setup.

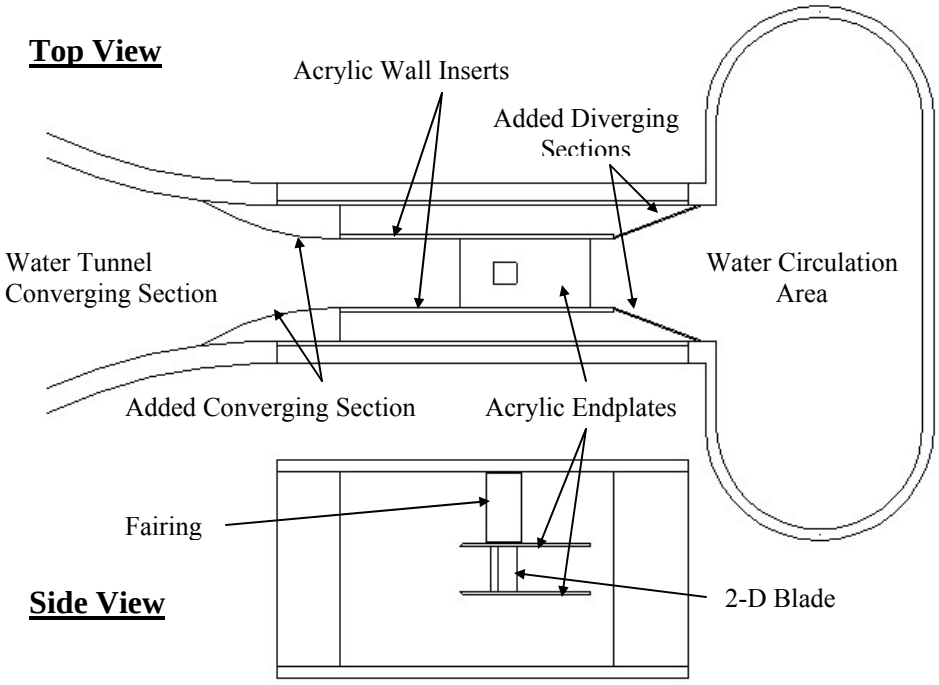

Figure 29: Schematic of Water Tunnel Setup

The acrylic inserts allow the flow to reach a velocity of 2 m/s in the test-section. Acrylic endplates were then installed between the two wall inserts to create the 2-D affect of an infinite blade. The endplates cancel out any 3-D affects that could distort the load data obtained during the tests. A fairing was created to shield the sting from the pressure exerted by the moving water. The fairing has the profile of a NACA 0014 and was built out of ABS plastic using a rapid prototype machine. The fairing slides into a hole created in the top endplate with the bottom of the fairing and endplate meeting flush. Screws are used to secure the fairing to the top endplate. The hole in the top endplate is the access point for the 2-D blade. Figure 30 and Figure 31 show the acrylic wall inserts, endplates, and fairing installed in the water tunnel test-section.

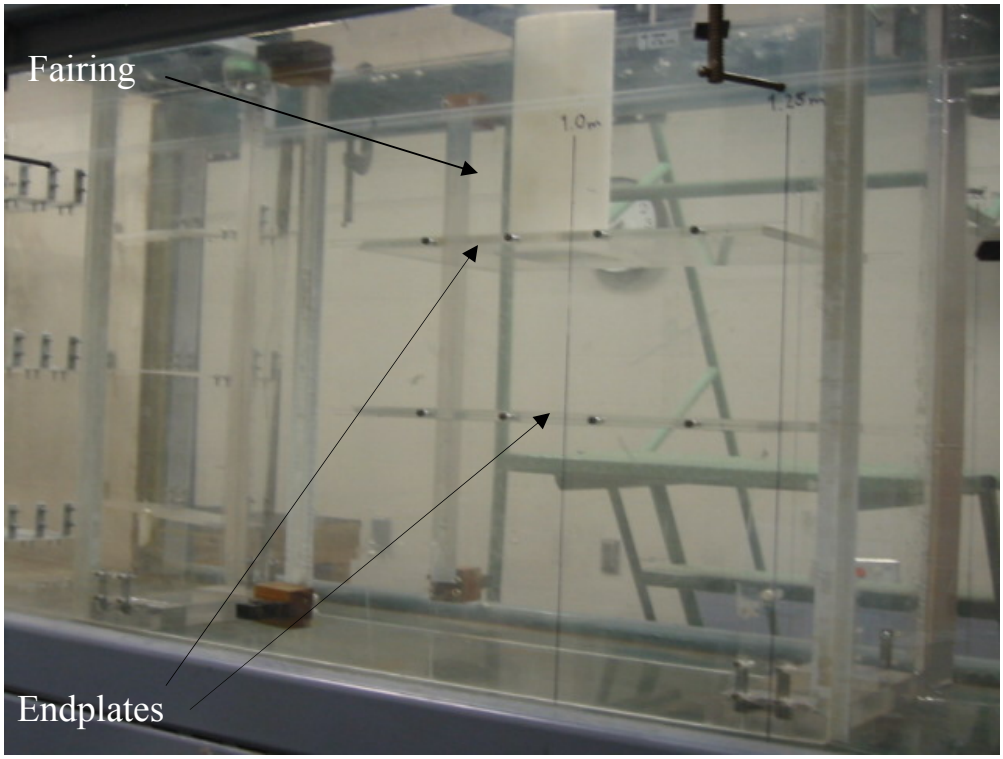

Figure 30: Side View of Acrylic Inserts with Fairing and Endplates

Figure 31: Through View of Acrylic Inserts with Fairing and Endplates

Water Tunnel Balance

To obtain the lift and drag on the 2-D blade, a balance was designed and built for mounting on top of the water tunnel test-section. The balance designed for the experiment has two axes, so that both lift and drag could be obtained simultaneously. Two pneumatic linear bearings from Nelson Air were used to minimize any frictional forces within the balance that could distort the load data.

One of the pneumatic linear bearings was mounted to the balance platform to allow an axis of motion parallel to the flow. A load cell was attached to the balance platform and the rear of the linear bearing for obtaining the drag generated by the presence of the blade. Attached to the other end of the drag bearing was a clamping mechanism, which held the sting. The sting is an aluminum rod 25.4 mm in diameter and 0.5588 meters in length that is attached to the 2-D blade. When loosened, the clamping mechanism would allow the sting to rotate. A plate with lines representing 1-degree angle increments was fastened to the drag bearing, on top of the clamping mechanism, so that the sting and blade could be adjusted to the correct angle of attack through the test matrix. The resolution of the angle of attack was 0.25° with a maximum uncertainty of 0.25°.

A second pneumatic linear bearing was mounted to the balance platform perpendicular to the drag bearing to allow for a second axis of motion. Support beams were mounted to the bearing to span the top of the water tunnel so the balance could be secured with clamps to prevent any movement during the test. A load cell was mounted to a support beam and the balance platform to obtain the lift generated by the blade. A 3-

D rendering of the balance that was created can be seen in Figure 32. Figure 33 shows a view of the actual balance on top of the water tunnel.

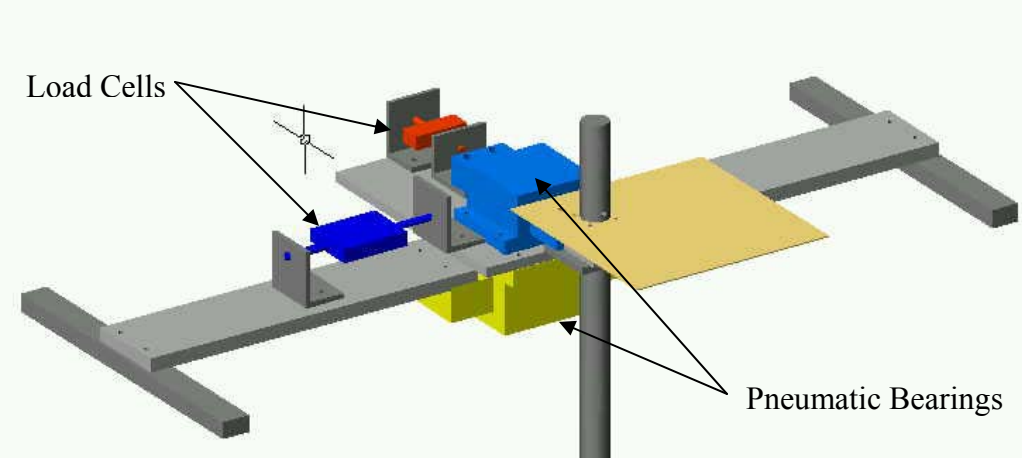

Figure 32: Balance with Sting

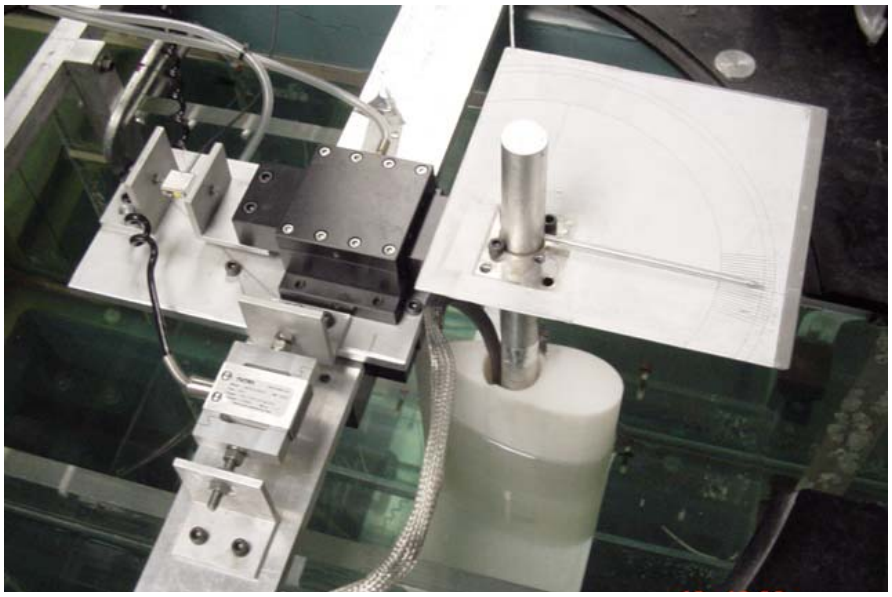

Figure 33: Top View of Water Tunnel Balance

Hardware Setup

Figure 34 shows a schematic of the experimental setup and how information and power was transferred for the load test and deflection test of the 2-D blade.

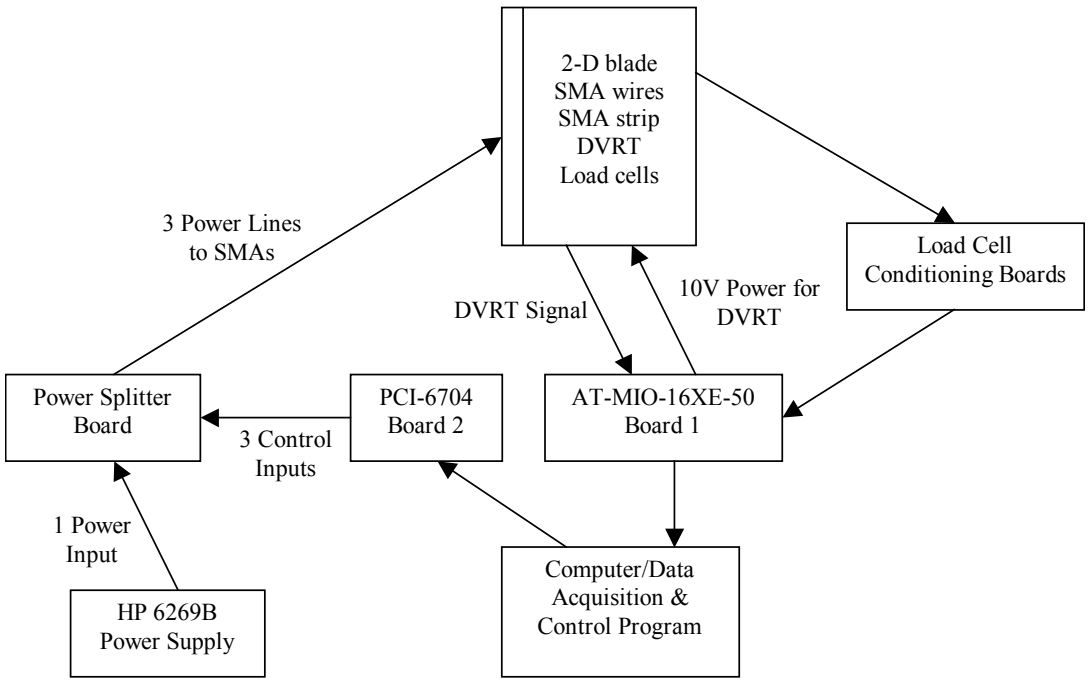

Figure 34: Schematic of Experimental Setup

Load Cells

Two load cells were used in the testing of the 2-D blade with leading edge flap. The load cell used for obtaining the lift was a Futek L2352 with a 111.21 N capacity and overload protection. The resolution of the lift was 0.004 N with an uncertainty of 0.05 N. The drag load cell was a Futek L2357 with a 8.896 N capacity and overload protection. The resolution of the drag was 0.0005 N with an uncertainty of 0.02 N. The output of

both load cells was conditioned using two Transducer Techniques TM0-1 Amplifier/Conditioner Modules.

Linear Displacement Sensor

A linear displacement sensor was mounted in the trailing edge cavity of the 2-D blade. The sensor is a waterproof Microstrain DVRT that gives a voltage output, which is linear to the displacement. The shaft of the sensor is attached to the leading edge flap by a hinge and was calibrated over a leading edge deflection range of -8° (up deflection) to +12° (down deflection). An equation given by Microstrain (Eqn. 1) was used to determine the reference position, P_{ref}, for a zero degree deflection and the current linear position, P_{cur}, where P is the position of the shaft and V is the voltage output from the sensor.

$$P = 1.37647 * V - 3.59326 \quad \textbf{(1)}$$

The reference position was subtracted from the current linear position to obtain the linear displacement, d (Eqn. 2).

$$d = P_{cur} - P_{ref} \quad \textbf{(2)}$$

An equation for converting the linear displacement of the sensor to an angular displacement was then used to determine the deflection angle of the leading edge (Eqn. 3). The equation is a 6th order polynomial with an R^2 of 0.9996. The actual deflection angle, A, is determined by the linear displacement, d.

$$A = 1322.1 * d^6 + 1085.1 * d^5 + 222.28 * d^4 + 13.458 * d^3 + 21.015 * d^2 + 28.85 * d \quad \textbf{(3)}$$

The leading edge deflection resolution was 0.01° with a maximum uncertainty of 0.02°. Figure 35 shows a picture of the Microstrain DVRT.

Figure 35: Microstrain DVRT Sensor

Power Supplies

The load cells used in the test were each powered by 12.0 volts supplied by the two Transducer Techniques TM0-1s, which used AC power adapters. The linear displacement sensor was powered by a fixed 10.0-volt output from a National Instruments A/D board. A Hewlett-Packard 6269B power supply was used for current input of the SMA wires, which has an operating range of 0-40 volts and 0-50 amperes.

Power Splitter Board

The power splitter board is a pulse-width-modulator, which takes a single input from the HP 6269B power supply and splits it into six individually controllable channels. The output is a current pulse with amplitude of V_C/R, where V_C is the input voltage from the HP 6269B power supply and R is the resistance of the output channel. The output of a channel is controlled by the duty cycle of that channel. The duty cycles are controlled by voltage inputs sent from the control program through a National Instrument A/D board. The design and manufacturing of the power splitter board was performed at the Texas A&M University Physics Electronics Shop.

Data Acquisition Boards

A National Instruments AT-MIO-16XE-50 A/D board was used to sample the voltages of both the linear displacement sensor and load cells and supply the needed 10-volts to power the sensor. The data acquisition board has a 16-bit resolution with eight differential input and two output channels. Three of the input channels and one of the output channels were used.

The control voltages used to alter the power splitter board output were sent through a National Instruments PCI-6704 A/D board. The data acquisition board has a 16-bit resolution with 16 differential output channels. Three out of the eight output channels were used.

Control Program

The control program created for the actuation of the leading edge was written in LabVIEW and is a Proportional/Integral control algorithm that contains closed loop feedback from the linear displacement sensor mentioned above. Eqns. 4-6 were used to determine the control values needed to actuate the leading edge flap, where *KP* and *KI* are the proportional and integral control gains respectively. These control gains were determined experimentally.

$$Err = DesAng - A \quad \textbf{(4)}$$

$$ErrInt = \int Err * dt \quad \textbf{(5)}$$

$$u = ErrInt * KI + Err * KP \quad \textbf{(6)}$$

$$DutyCycle = \sqrt{u} \quad \textbf{(7)}$$

In Eqn. 4, the current angle deflection, A, was compared to the desired angle, DesAng, to obtain the amount of real time error, Err. For this program, the acceptable error was set to 0.1 degrees to terminate actuation of the leading edge. ErrInt is the sum of Err over the amount of time taken for actuation. The control, u, in Eqn. 6 determined the amount of power sent to the SMA wires. The duty cycle for the channel being actuated was set using Eqn. 7. If the leading edge flap angle produced a negative error due to overshoot, the control and duty cycle were set to zero. The SMA would then cool down and regress back to a positive error where actuation would continue until the required error was met.

RESULTS AND DISCUSSION

Flow Angularity

A 2-D blade with the profile of a NACA 0012 was built to see if the flow through the reduced test section contained any flow angularity. The blade was 0.2032 meters in span as the 2-D blade with leading edge flap and was made out of ABS plastic using a rapid prototype machine. The blade was placed in the water tunnel using the same sting and balance configuration stated above. A load test was conducted to obtain the lift on the blade. An angle of attack sweep from -10° to 10° was performed. Figure 36 shows a plot of the results from the load cell. From the plot it can be seen that the data is fairly linear and goes through zero. With this knowledge it can be assumed that there is no flow angularity present in the test section. Due to the angle of attack being adjusted by hand and angle verified by eye, uncertainty in the data is present.

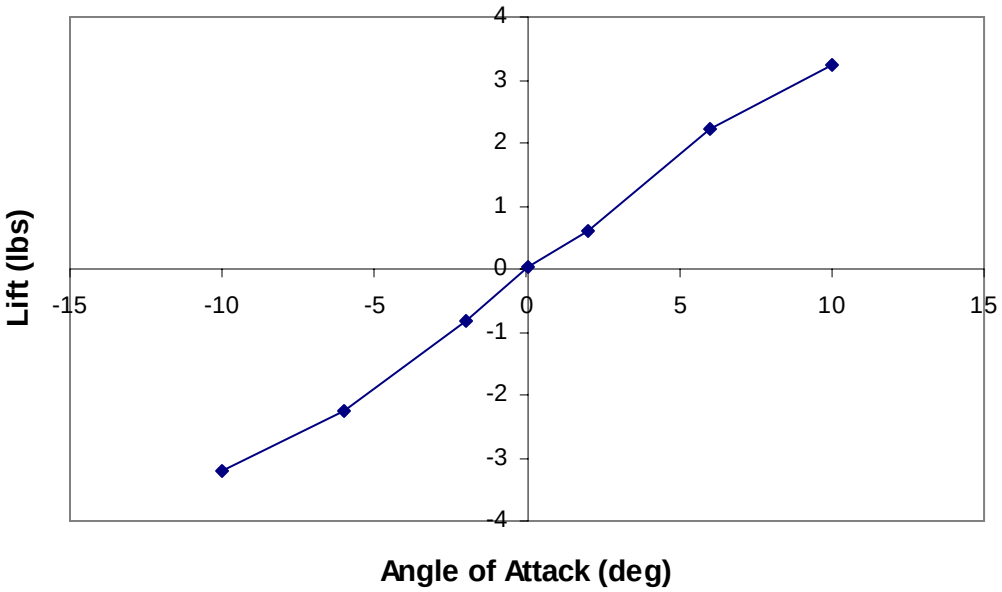

Figure 36: Lift vs. Angle of Attack for NACA 0012

2-D Blade with Leading Edge Flap

Load Test

The purpose of the load test on the 2-D blade was to obtain the lift and drag for different angle of attack and flap deflection combinations. The data allowed us to see how the presents of the leading edge flap would alter the blade loading on the propeller in the region of 70% span. For this test, leading edge deflection was not obtained by SMA actuation due to technical difficulties associated with noise. The high currents required to actuate the leading edge produced noise, which interfered with the signal from the linear displacement sensor housed within the blade cavity. The magnitude of the noise experienced during actuation was twice the acceptable error, so actuation of the leading edge would not terminate. To temporarily side step the issue, the leading edge was adjusted by hand and locked into place using the screws spanning the flap. The deflection angle was set using the Microstrain DVRT. Once the leading edge was locked into place, an angle of attack sweep of -10° to 10° in increments of 2° was performed. The water velocity within the reduced test section was set at approximately 1.2 m/s. Figure 37 is a picture of the 2-D blade in the water tunnel during the load test.

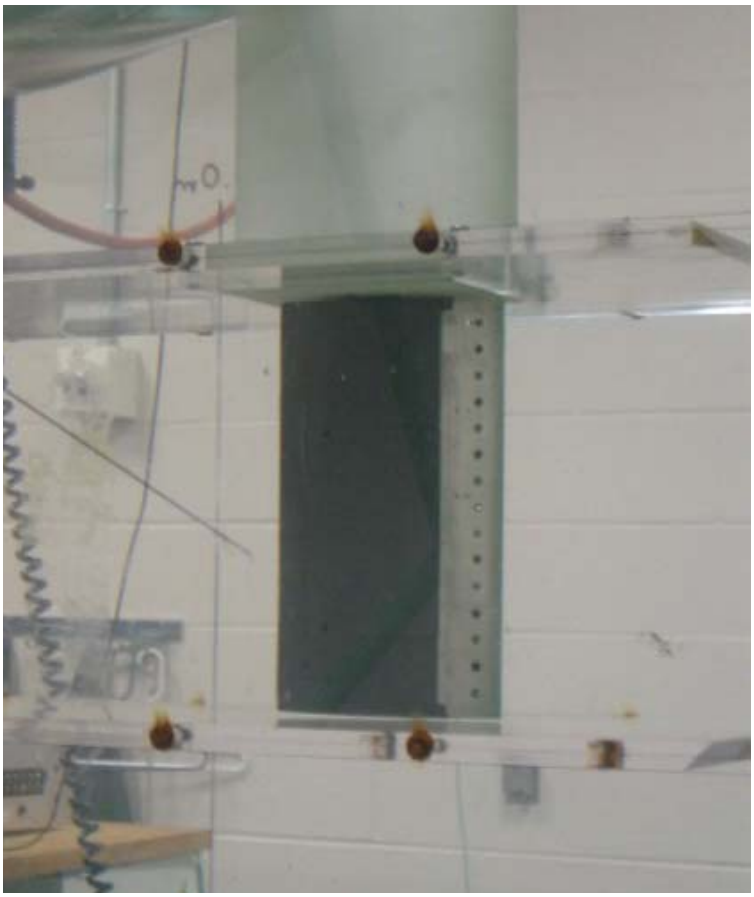

Figure 37: 2-D Blade in Water Tunnel During Testing

The lift and drag for each configuration was obtained by taking the mean value of 10,000 data points at a rate of 1,000 points per second. Figures 38 and 39 show the load data obtained during the test. It can be seen from the graph, in the outer limits of the angle of attack range, that the lift increases with increasing positive deflection (leading edge down) of the flap. This increase in lift is expected due to the positive flap deflection increasing the camber of the blade. Problems were encountered with the drag load cell at high positive angles of attack. The signal would not stabilize and underwent a series of step function fluctuations. It is not clear what the cause of the problem was, but it is speculated that the conditioning board might have malfunctioned.

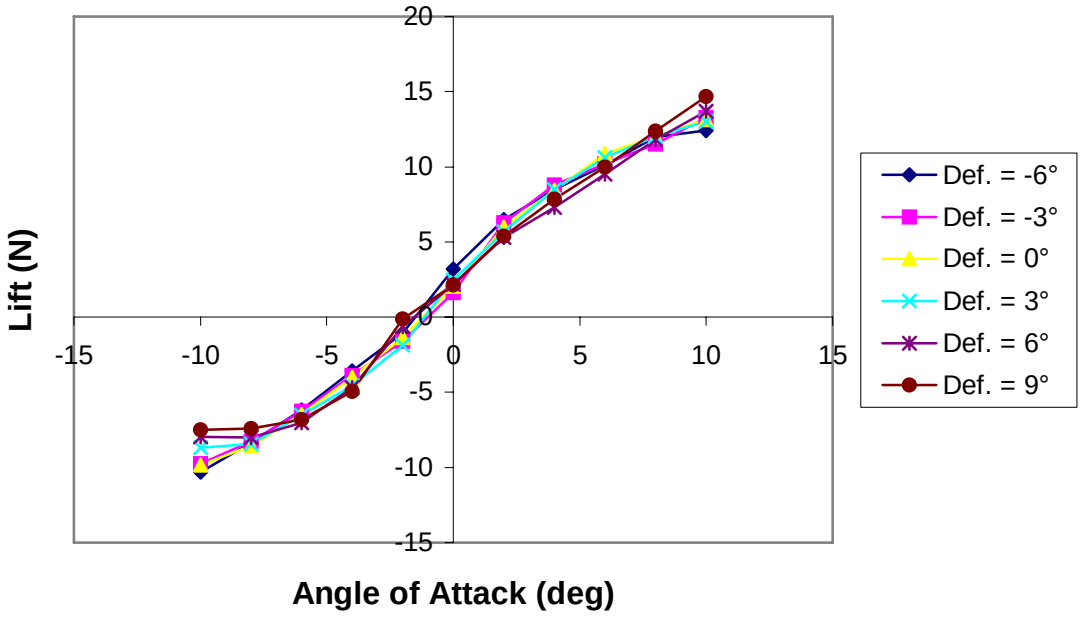

Figure 38: Lift vs. Angle of Attack of 2-D Blade for Increasing Flap Deflection (Def)

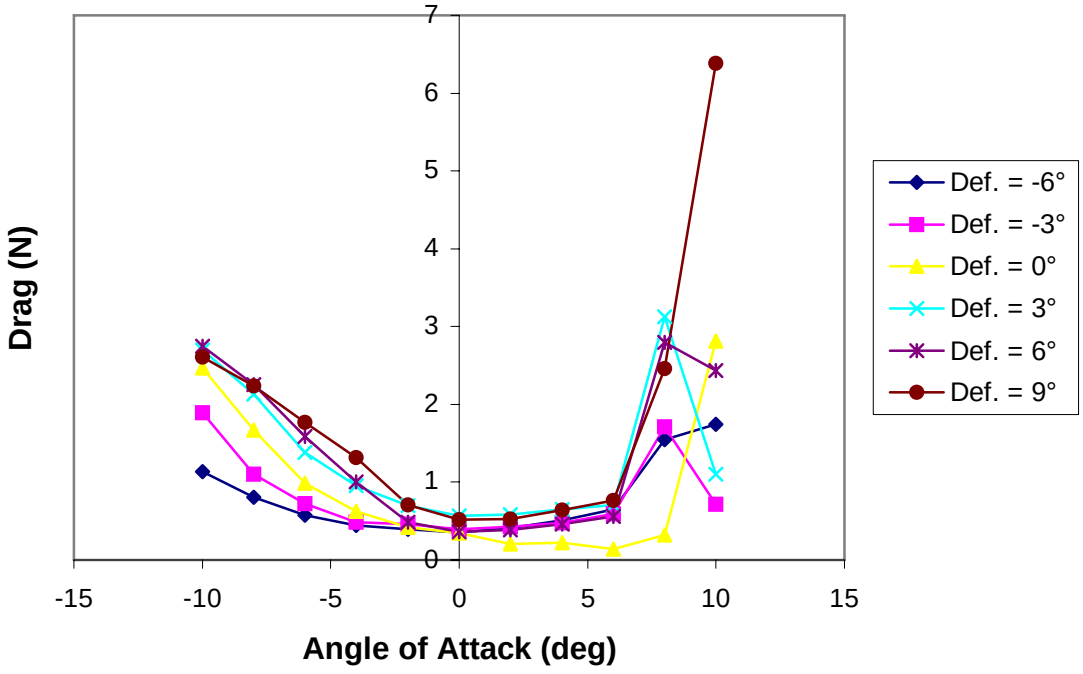

Figure 39: Drag vs. Angle of Attack of 2-D Blade for Increasing Flap Deflection (Def)

Leading Edge Deflection

Deflection of the leading edge was achieved using the SMAs housed within the 2-D blade in still water conditions. Step inputs were used to deflect the leading edge to the desired angle of attack. A voltage input of 16 volts was sent to the power splitter board via the HP 6269B power supply for actuation of the leading edge. The linear displacement sensor in the blade provided feedback to the control program. Output from the sensor was sent through a butterworth lowpass filter with a cutoff frequency of 30.0 Hz to reduce the noise generated from the wires used for power transmission. Deflection cycles of approximately 0.016 Hz were encountered during the test for deflections of 1°. A leading edge deflection of 5 degrees was obtained for positive deflection (leading edge down) and –2.5 degrees for negative deflection (leading edge up). The clamping force generated by the leading edge was found to be inadequate for holding the larger deflection angles. It was also found that the locking and releasing mechanism contained within the leading edge could not reduce the clamping force along the entire span of the blade having one point of contact with the walls. A frictional force about the shaft would develop as deflection of the leading edge increased which reduced the effectiveness of the clamping. Figure 40 shows the leading edge at 0.0 degrees (left) and –2.5 degrees (right) deflection angle actuated by SMA with the low pass filter.

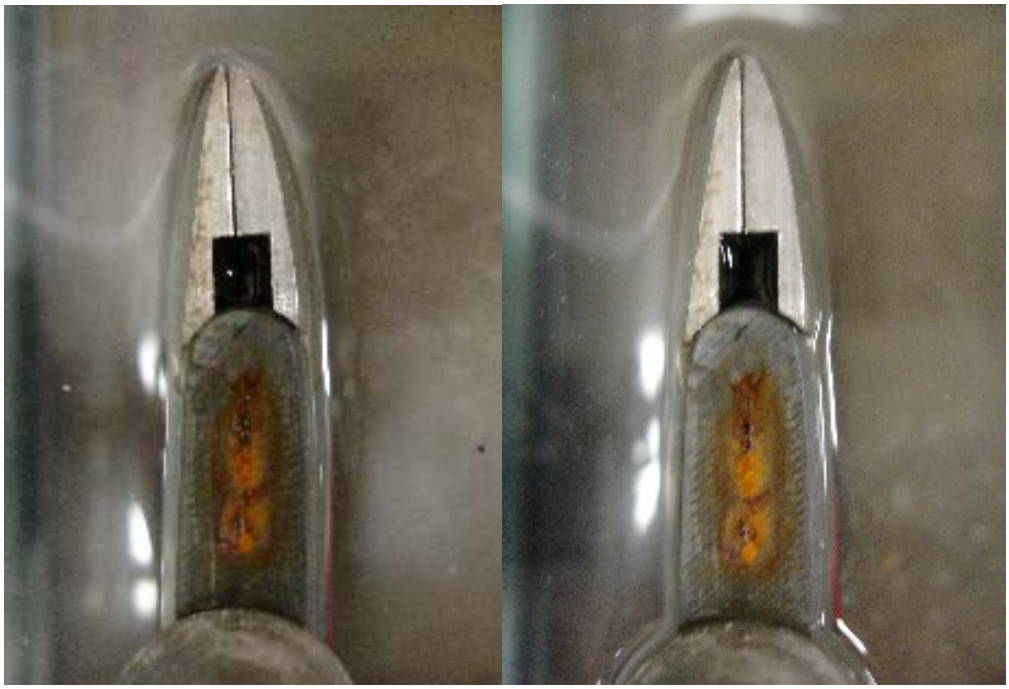

Figure 40: Leading Edge at 0.0 Degrees (Left) and -2.5 Degrees (Right)

Tracking of the leading edge flap was performed for both positive and negative deflections. Figures 41 and 42 show the results of the tracking of step inputs for positive and negative flap deflections respectively.

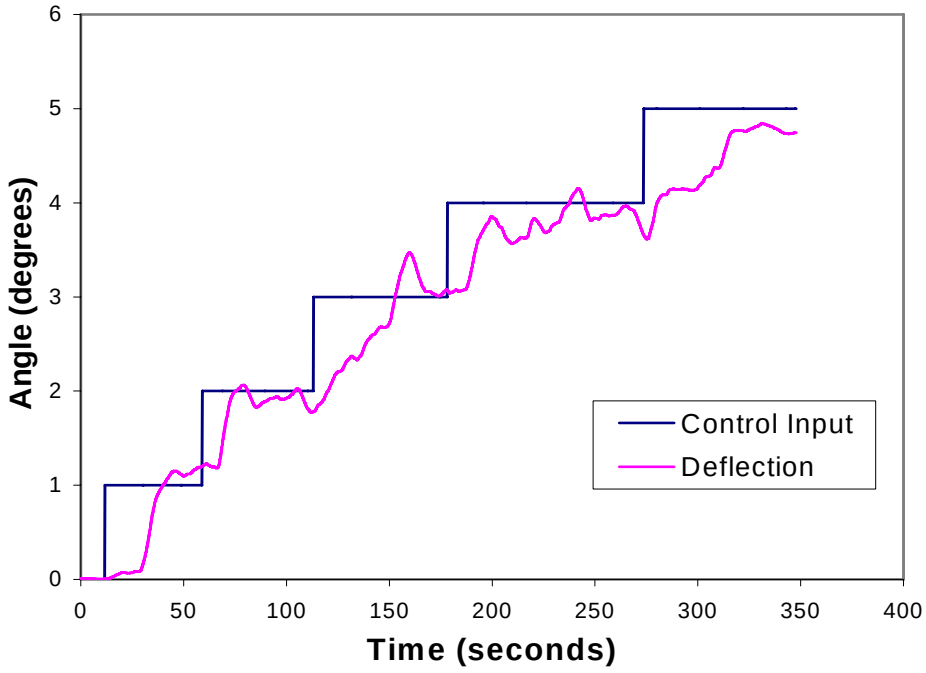

Figure 41: Positive Deflection Trace of Leading Edge Flap

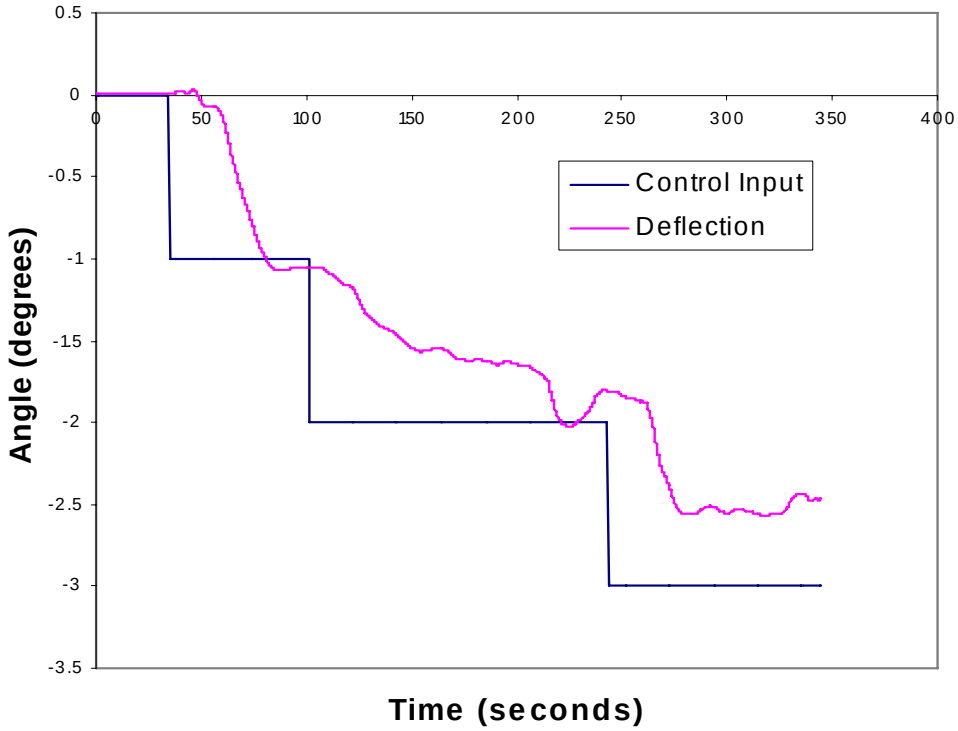

Figure 42: Negative Deflection Trace of Leading Edge Flap

PRELIMINARY DESIGN OF 3-D PROPELLER

The last stage was the preliminary design of a 3-D propeller. The data files given to Texas A&M University, which contain the outer surface of the blade, were used to create a solid model of the propeller in Solid Works. Due to the equipment available at Texas A&M University and the possible difficulties in manufacturing if future work is done, the propeller has only two blades and a diameter of approximately 0.3048 meters. The power splitter board used to actuate the SMAs located in the propeller has six channels and with the current design each blade requires three channels. Two blades are all that can be powered without having a new power splitter board built. The blades have a leading edge flap 0.0381 meters in length and are centered at about 70% of the span. The hub of the propeller contains a slip ring system to transfer electricity from the power source to the SMAs. Commercial slip rings that meet the specifications required for leading edge actuation are available through companies such as Moog Components Group. A possible design for a simplified slip ring system using aluminum rings is described below. Wires are attached to the slip ring system and run through holes in the propeller blades to the SMAs. Figures 43 and 44 show a 3-D rendering of the propeller currently created in Solid Works.

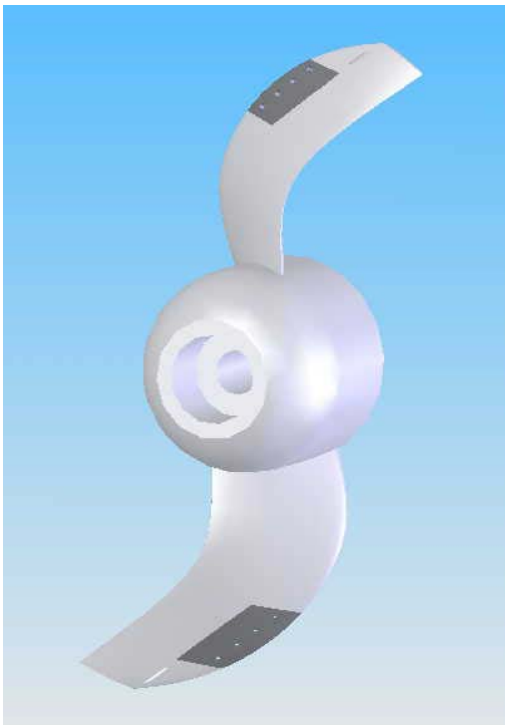

Figure 43: 3-D Rendering of Propeller, Pressure Side

Figure 44: 3-D Rendering of Propeller, Suction Side

For the simplified design, aluminum slip rings are placed concentrically about the propeller shaft with insulating rings made of phenolic between each aluminum ring. The phenolic rings extend past the aluminum rings to create channels for mating with the other half of the slip ring system contained in the shaft housing. Figure 45 shows a 3-D rendering of the slip ring concept contained within the hub.

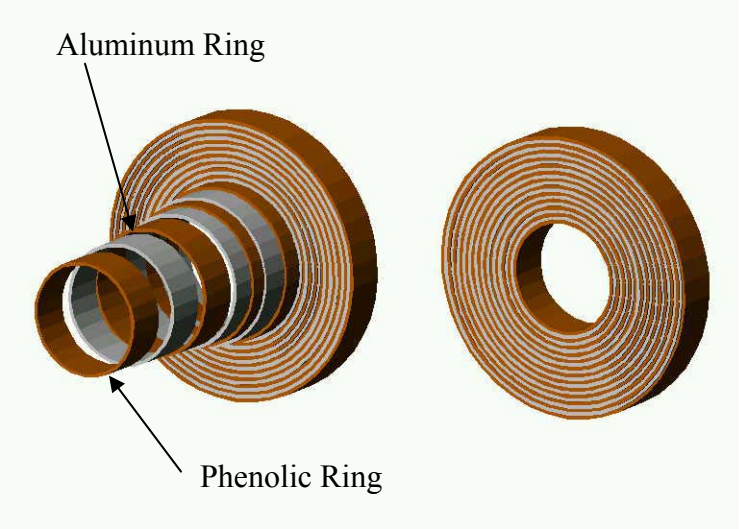

Figure 45: Aluminum and Phenolic Slip Rings

The shaft housing has an identical slip ring setup as the propeller hub with the aluminum rings extending past the phenolic rings. Brushes are attached to the aluminum rings within the shaft housing to assure continuous solid contact with the slip rings within the propeller hub.

CONCLUSION AND RECOMMENDATIONS

Conclusion

A study was performed to investigate the feasibility of using Shape Memory Alloys as part of an active control system for altering the geometry of a propeller blade by deflection of a leading edge flap. The flap was designed with an internal shaft locking and releasing mechanism so that constant actuation of the SMAs would not be required to maintain leading edge deflection. The design of the leading edge flap was implemented in a 2-D blade that spanned 0.2032 meters with the profile of the propeller blade at 70% span. Deflection cycles of approximately 0.016 Hz were encountered during testing. A leading edge deflection of 5 degrees was obtained for positive deflection (leading edge down) and –2.5 degrees for negative deflection (leading edge up). It was found that the force generated by the locking and releasing mechanism was inadequate for larger deflection angles. After actuation stopped, the flap would regress back to a smaller deflection angle where actuation would then be readmitted by the control program. It was also found that the locking and releasing mechanism contained within the leading edge could not reduce the clamping force along the entire span of the blade having one point of contact with the walls. A frictional force about the shaft would develop as deflection of the leading edge increased which reduced the effectiveness of the clamping.

From the load data obtained during the water tunnel test, it can be seen at the outer limits of the angle of attack range, that the lift increases with increasing positive deflection (leading edge down) of the flap. This change in lift assures that a leading edge

flap on a propeller blade can be used to alter the blade loading. The change in blade loading will allow for a decrease in rotational speed of the propeller and in turn a reduction in radiated noise. During testing, problems were encountered with the drag load cell at high positive angles of attack. The signal would not stabilize and underwent a series of step function fluctuations. It is not clear what was the cause of the problem, but it is speculated that the conditioning board might have malfunctioned.

Using the design of the leading edge flap and locking and releasing mechanism, a preliminary design for a 3-D propeller was created. The propeller has two blades and a diameter of 0.3048 meters. The blades have a leading edge flap 0.0381 meters in length and are centered at 70% span. The hub of the propeller contains insulated slip rings made of aluminum to transfer electricity from the power source to the SMAs. Wires are run from the aluminum slip rings through holes in the propeller blades to the SMAs.

The research has shown that active cambering by deflection of a leading edge flap utilizing SMA actuators can be used to change the blade loading on a propeller.

Recommendations

The drag load cell experienced problems during the load test for high angles of attack. The signal was irregular and it is suggested that the conditioning board be examined for possible causes. The conditioning board may need to be recalibrated, or exchanged for a new one. The signals of both load cells contained a great deal of noise through the entire angle of attack range. The implementation of lowpass butterworth filters may eliminate or reduce the magnitude of the noise.

The leading edge flap needs to be modified to ensure that adequate force is available for clamping onto the shaft so that large angle deflections can be held. The

leading edge could be made out of stainless steel so that the screws running the span of the blade can be tightened without fear of stripping the threads. The locking and releasing mechanism could not release the clamping force evenly along the complete span of the blade with one contact point. The locking and releasing mechanism needs to be redesigned with multiple contact points spaced along the span of the flap.

The trailing edge blade section needs to be built out of aluminum or stainless steel to ensure that the structure is rigid enough to withstand the forces generated by the SMAs. This change will help prevent warping of the blade. The cavity of the trailing edge may need to be redesigned to house longer SMAs so that larger strains and in turn larger deflections of the leading edge can be obtained. The longer SMAs will also reduce the amount of stress experienced by the material itself. If possible, the moment arm for actuation of the leading edge needs to be increased to allow for a greater range of deflection. The hinges used to clamp onto the SMA wires need to be redesigned or built out of steel so that the forces holding the wires are large enough that the SMA does not come loose during actuation.

REFERENCES

[1]Taggart, R., "Marine Propulsion Principles & Evolution," Gulf Publishing Company: Austin, Texas 1969, pp. 222-232

[2]Bandyopadhyay, P. R., Krol, W. P., Jr., Thivierge, D. P., Nedderman, W. H., and Mojarrad, M., "A Biomimetic Propulsor for Active Noise Control. Part 1: Experiments," Bulletin of the American Physical Society, Vol. 45, No. 9, 2000

[3] Bandyopadhyay, P. R., Krol, W., Thivierge, D. P., Nedderman, W. H., and Mojarrad, M., "A Biomimetic Propulsor for Active Noise Control: Experiments," NUWC-NPT Technical Report 11,351, Newport, Rhode Island, March 2002

[4]Quackenbush, T. R., and Usab, W. J., Jr., "Ducted Propulsors with Steerable Outflow Using Smart Materials," Continuum Dynamics Inc., www.continuum-dynamics.com/research/ topics/variable_geometry_ducted_prop/smartductpaper.pdf

[5]Hess, D. E., and Fu, T. C., "Impact of Flow Control Technologies on Naval Platforms," Paper No. AIAA 2003-3568, 33rd AIAA Fluid Dynamics Conference, June 2003, Orlando, Florida

[6]Annaswamy, A. M., Krol, W. P., Jr., and Bandyopadhyay, P. R., "A Biomimetic Propulsor for Active Noise Control. Part 2: Theory," Bulletin of the American Physical Society, Vol. 45, No. 9, 2000

[7]Singh, K., and Chopra, I., "Design of an Improved Shape Memory Alloy Actuator for Rotor Blade Tracking," SPIE Paper No. 0277-786X, Proceedings of SPIE Vol. 4701, 2002

[8]Straub, F. K., and Merkley, D. J., "Design of a Smart Material Actuator for Rotor Control," Smart Mater. Struct. 6, 1997, pp. 223-234

[9]Kennedy, D. K., Straub, F. K., Schetky, L. M., Chaudhry, Z., and Roznoy, R., "Development of an SMA Actuator for In-flight Rotor Blade Tracking," *Journal of Intelligent Material Systems and Structures*, Vol. 15, April 2004, pp. 235-248

[10]Gowing, S., Carpenter, B., Atsavapranee, P., Lee, Y., Lee, M., and Hess, D., "FlexTAC: Flexible Tab Assisted Control for Submarine Application," NSWC Research & Development Report, NSWCCD-50-TR-2003/029, June 2003

[11]Rediniotis, O. K., Lagoudas, D. C., and Wilson, L. N., "Development of a Shape Memory Alloy Actuated Underwater Biomimetic Vehicle," AIAA Paper No. 2000-0522, 38th Aerospace Science Meeting and Exhibit, January 2000, Reno, Nevada

[12] Rediniotis, O. K., and Lagoudas D. C., "Shape Memory Alloy Actuators as Locomotor Muscles in Fixed and Flapping Wing Aerodynamics for Micro Air Vehicles", ed. Thomas J. Mueller, *Progress in Aeronautics and Astronautics*, Vol. 195, published by AIAA, Nov. 2001, pp. 483-500

[13]Webb, G., Wilson, L., Lagoudus, D., and Rediniotis, O., "Control of SMA Actuators in Dynamic Environments," SPIE Paper No. 3667-99, SPIE's 6th Annual International Symposium on Smart Structures and Materials, March 1999, Newport Beach, California

[14]Lin, R., "Shape Memory Alloys and Their Applications", Stanford University, http://www.stanford.edu/~richlin1/sma/sma.html, 1998, accessed on Jul. 17, 2005

[15]Shape Memory Alloys, eSMART, http://www.cs.ualberta.ca/~database/MEMS/sma_mems/sma.html, 2001, accessed on Jul. 17, 2005

VITA

Name: Jonathan Wasylyszyn

Address: H.R. Bright Building, Rm. 701, Ross Street - TAMU 3141
College Station TX 77843-3141

Education: B.A., Aerospace Engineering, Texas A&M University, 2003
M.S., Aerospace Engineering, Texas A&M University, 2005